THE PENNSYLVANIA
STATE UNIVERSITY

A MODULE FOR AUTOMATIC DOCK AND DETUMBLE (MADD) FOR ORBITAL RESCUE OPERATIONS

BY

WILLIAM R. SNOW
BOHDAN G. KUNCIW
MARSHALL H. KAPLAN

ASTRONAUTICS RESEARCH REPORT
NO. 73-3

DEPARTMENT OF AEROSPACE ENGINEERING
UNIVERSITY PARK, PENNSYLVANIA

APRIL 1973

RESEARCH SUPPORTED BY NASA GRANT NGR 39-009-210

Table of Contents

ABSTRACT

The Module for Automatic Dock and Detumble (MADD) is an automated device for bringing a passive, tumbling space base under control in an orbital rescue situation. The conceptual design of such a device resulted from a consideration of tumbling motion analyses and mission constraints. Specific topics of investigation include orbit and attitude dynamics and detumble profiles. Position and attitude control systems for the various phases of operation were developed. Dynamic motion of a passive vehicle with MADD attached is considered as an example application and to determine control requirements. Since time is a critical factor in rescue operations, it is essential to execute the detumbling maneuver in a minimum of time. Optimization of the MADD thrusting sequence has also been investigated. Results indicate the control torque must be directed opposite to the angular momentum vector for the assumptions used here.

List of Figures

Nomenclature

A, B, C	principal moments of inertia of MSS
$\underline{E}$	3 x 3 direction cosine matrix defining the actual orientation of MADD with respect to the command orientation (error matrix)
p, q, r	angular velocities in a right hand system
$\underline{A_{as}}$	3 x 3 direction cosine matrix defining the attitude of MADD with respect to the moving coordinate frame
$\underline{A_{cs}}$	3 x 3 direction cosine matrix defining the command attitude for MADD with respect to the moving coordinate frame
$\bar{a}_i$	unit orthogonal vectors attached to the body fixed axes of MADD defining its coordinate frame, $(i = 1,2,3)$
$\bar{b}_i$	components of the eigenvector b in the body roll, pitch, and yaw axes, respectively, $(i = x,y,z)$
$\bar{c}_i$	unit orthogonal vectors defining the command attitude of MADD, $(i = 1,2,3)$
I_i	moments of inertia of MADD, $(i = x,y,z)$
K_{Ai}	gain terms associated with the control law about the body roll, pitch, and yaw axes $K_{Ai} = [I_i\ L(max)/I(max)]$ $(i = x,y,z)$
K_B	rate gain term associated with the control law, $1/w_a(max)$
L_i	values of control torque, $(i = x,y,z)$
$\bar{S}_i$	unit orthogonal vectors defining the moving (reference) coordinate frame, $(i = 1,2,3)$
β	angle of rotation about the axis which is the eigenvector of the $\underline{E}$ matrix
δ	gimbal angle
β_s	value of β at which L_i saturates

ψ_a, ϕ_a, θ_a	Euler angles of the actual attitude of MADD
ψ_b, ϕ_b, θ_b	Euler angles of the MSS body fixed axes
ψ_c, ϕ_c, θ_c	Euler angles for the command attitude coordinate frame.
ω_{ai}	actual MADD body angular rates relative to the moving coordinate frame, (i = x,y,z)
ω_i	MSS angular rates about principal axes, (i = 1,2,3)
Ω	gyro angular velocity

I. Introduction

In the operation of any manned space vehicle there is a small but finite probability that an accident will render it disabled and tumbling. It is probable that such a vehicle must be detumbled before evacuating the crew and repairs can be performed. "Tumbling" is the result of a significant attitude perturbation to an uncontrolled body. This results in continuous angular motion about all three principal body axes, i.e., no inertially oriented axis. The vehicle would reach a stable spin after a sufficient amount of energy is dissipated, but this might take many weeks or months for a large craft. Astronauts trapped in such a body could not easily escape.

Situations that are most likely to cause tumbling are collision, malfunctioning thruster, and escaping stored gas or liquid. From a worst case analysis, estimated tumble rates of a large modular space station (MSS) are as high as 2 RPM about the principal axes.[1] Elimination of angular motion must be done from the nontumbling frame of the shuttle orbiter. A Module for Automatic Dock and Detumble (MADD) would perform an orbit transfer from the shuttle and then execute a docking maneuver with the vehicle. Internal devices could be employed to reduce tumbling to simple spin. However, MADD is adaptable to various situations and can be used for the simplified case (spin) but only the general case (tumbling) is treated here. Once docked MADD will apply torques by firing its thrusters to detumble the craft. This will be done in a time optimal manner. Then the crew can be rescued and the mission completed.

II. Description of MADD

The purpose of MADD is to detumble a large passive space base. The MSS will be used as a realistic example with initial tumbling at an equivalent rate of about 2 RPM. Conceptual design of MADD was influenced by shuttle mission objectives and systems constraints. This module must be able to maneuver about, dock with, and detumble the MSS with a limited amount of fuel for various tumbling situations. The size of MADD is limited by the need for manuverability and shuttle specifications, 29,500 Kg (65,000 lb) payload and payload bay 18.3 m (60 ft) long by 4.5 m (15 ft) in diameter.[2] The size is also somewhat dependent upon the configuration of the target vehicle.

It is necessary that the CM of MADD remains fairly well fixed as fuel is consumed and that moments of inertia change little during transfer to simplify control requirements. Therefore, the fuel tanks should be located as to minimize this effect. The body frame should coincide with the principal axes to simplify control requirements, and thrusters should be far enough from the CM to minimize attitude propellant usage during transfer, but not so far as to put excessive moments on the docking mechanism during detumbling. MADD must have full orbit and attitude control for transfer to the target. A preliminary configuration for this device is shown in Figure 1.

The structure of this vehicle contains all subsystems with the docking probe mounted beneath and docking drogue mounted above the main structure, which is a 2.74 m (9 ft) octagon and is 1.22 m (4 ft) deep. This contains propellant (hydrazine) storage tanks, control systems, batteries, thrusters, and twin-gyro controllers. Subsystems

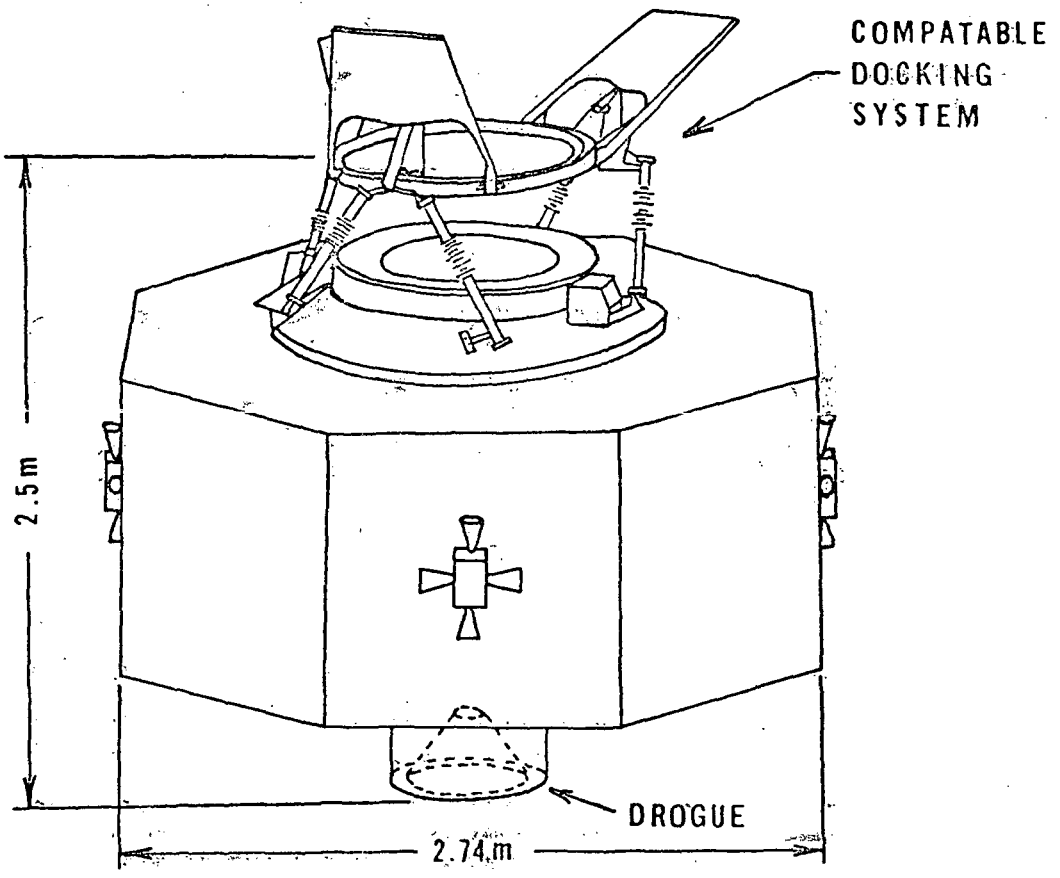

Figure 1. Details of MADD Configuration

include structure, digital computer, command and telemetry, power supply, control systems, guidance, and docking aids. The power supply will consist of storage batteries. Control systems consist of three types: position, attitude, and detumble. The position and attitude control systems provide maintenance of orientation and position during transfer and docking. Twin-gyro controllers and thrusters were chosen for attitude control devices. Monopropellant hydrazine thrusters were chosen for position control, detumbling, and momentum dumping, because of handling properties, specific impulse, and proven reliability.[3] During docking and detumbling the twin-gyro controllers will be locked. Once the disabled vehicle is detumbled, the twin-gyro controllers may be given new reference signals and released, and the position control system may be reactivated. Thrusters used for position control are also used for detumbling and attitude control. This was done to eliminate the need for separate systems of thrusters, even though there are three separate control systems. The thrust profile during the detumbling procedure is computed by the on-board computer according to the rules of optimum detumbling logic. The guidance system consists of an inertial platform that provides information on position and orientation of MADD, and rate gyros provide body rate information.

Docking aids consist of laser radar and corner reflectors and these are discussed further in the next section. The docking apparatus consists of two separate systems; one for a space base and one for the shuttle. A MADD docking probe is used to dock with one of the docking ports of the target vehicle, e.g., one located at the extremities of

the MSS modules. Capture latches are activated automatically after alignment. The shuttle docking systems consists of a remote-controlled manipulator boom, probe, capture latches, and a docking droque, which is controlled by shuttle crewmen. MADD is positioned about the shuttle as illustrated in Figure 2. It is then released to perform the mission, afterward the manipulator boom is used to retrieve MADD and stow it in the payload bay.

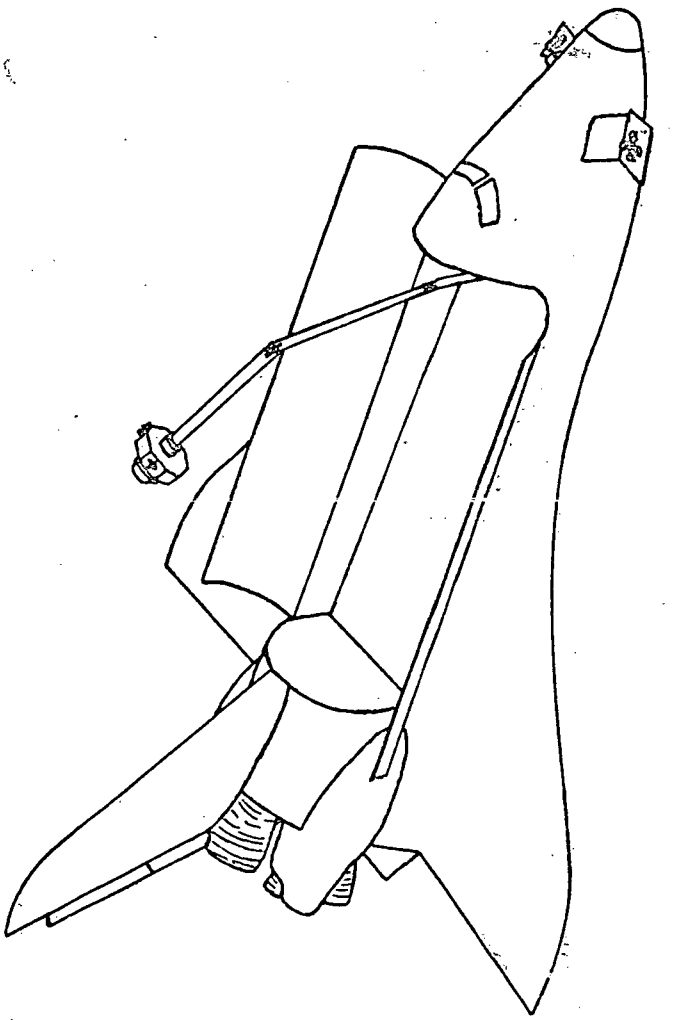

Figure 2. MADD Deployment Arrangement

III. Operational Procedure

Rescue operations begin as the shuttle completes its rendezvous with the distressed vehicle. The MSS will be used to illustrate the procedures. A typical rendezvous is shown in Figure 3. It is assumed that the methods required to locate the MSS, determine angular rates and momentum are available to the shuttle crew. A stand-off position will be established approximately 61 m (200 ft) away and along the orbital path. Mission profile for MADD after deployment from the cargo bay can be broken down into three phases: (1) thrust-free orbital transfer to a rendezvous point; (2) thrusted pacing with the docking port and docking; and (3) detumbling of the MSS. MADD becomes automatic at the rendezvous point and data is telemetered to the shuttle. Radio and visual contact may be lost intermittently because of occultation.

The rendezvous point is chosen so that the velocity vector at the instant MADD reaches it, will coincide with the velocity vector in the MSS moving coordinate frame. This would eliminate the need for a terminal maneuver to reorient the velocity vector, (they should coincide) and also reduce the risk of a collision with the MSS. Another constraint is that the trajectory must not allow MADD to collide with the MSS on its way to the rendezvous point. The actual transfer to the rendezvous point may require several impulses and corrections. An ideal transfer would require only one impulse. At the rendezvous point MADD should be approximately 4.6m (15 ft) away from the docking port. Thrusters begin firing to keep pace with the docking port maintaining proper

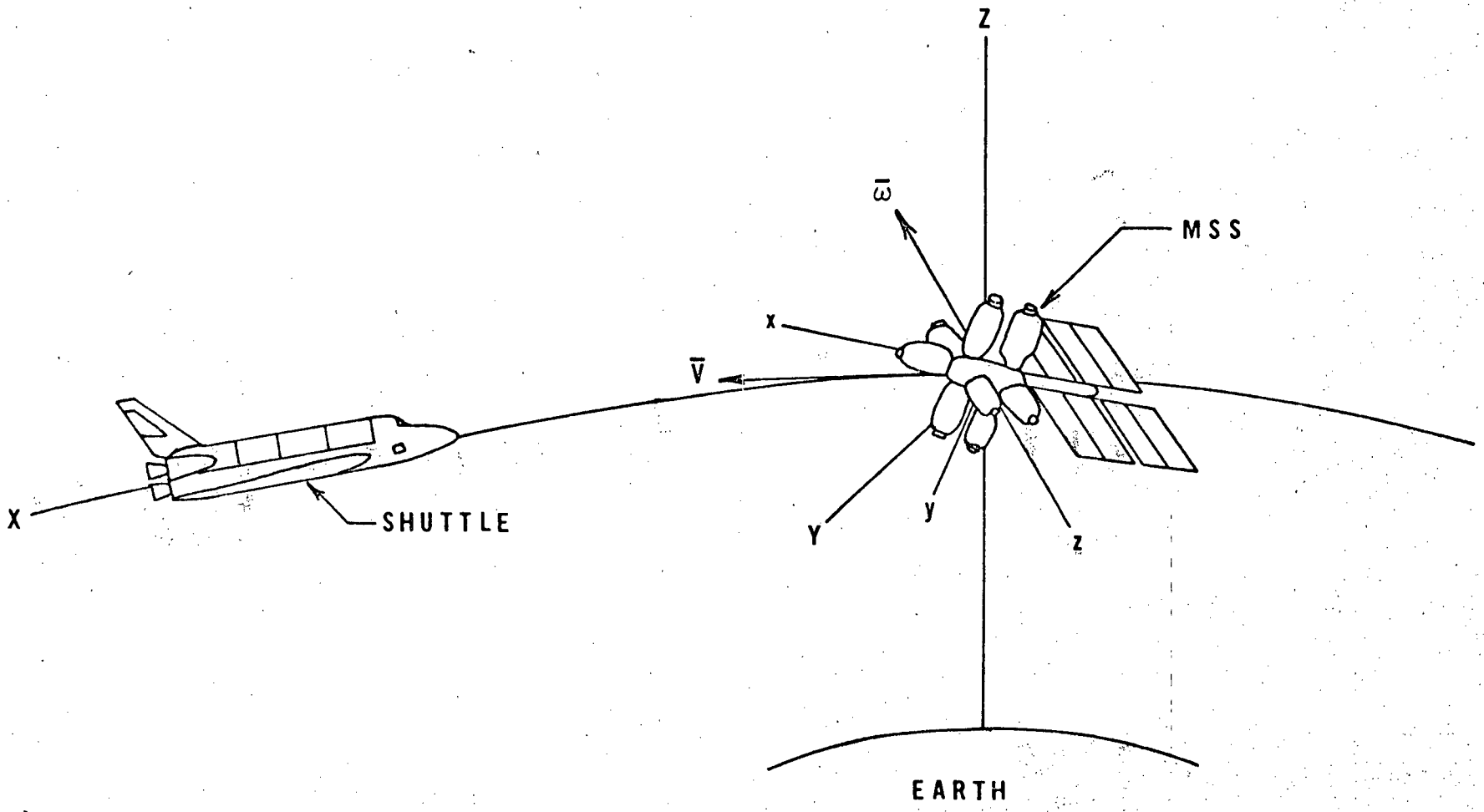

Figure 3. Shuttle/MSS Relative Position Nomenclature

position and attitude, while closing into dock (shown in Figure 4).

Automated rendezvous and docking is provided by a laser radar located on MADD and corner reflectors located on the docking port of the MSS.[4] MADD carries a transceiver that provides range, range rate, angles, and angular rates with respect to the docking port. This radar uses CW (continuous wave) modulation of an incoherent gallium arsenide injection diode laser. Acquisition occurs when MADD reaches the rendezvous point, at this point the system will be turned on and it will recieve signals from its own transmitter reflected back by corner reflectors located on the docking port. This permits proper alignment during closure and docking by providing guidance information. MADD continues closure until the docking probe has engaged and capture latches are secured.

Once docked angular rates are measured, and a thrust profile is computed. Thrusters can then detumble the MSS quickly, and rescue is completed.

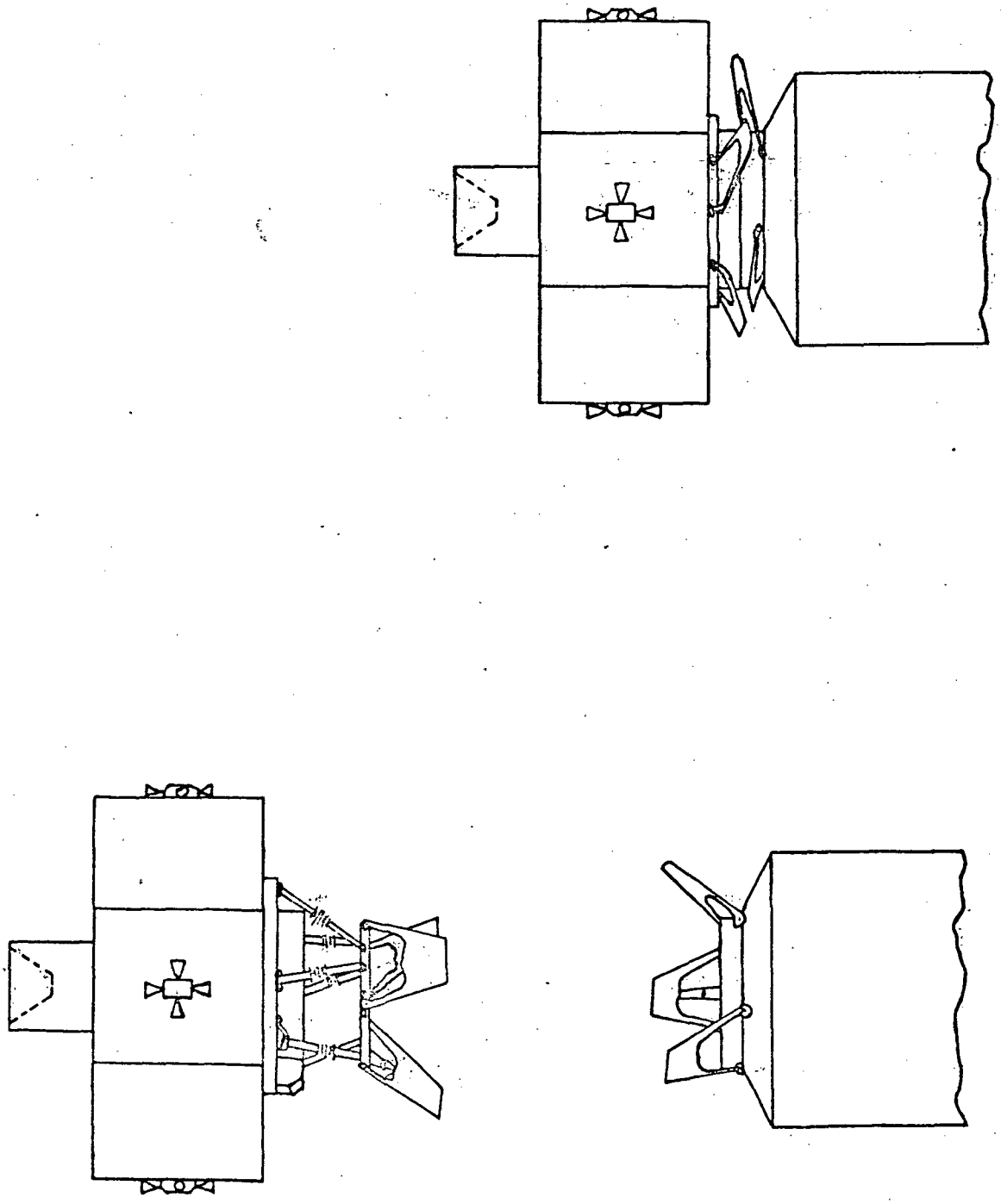

Figure 4. Rendezvous and Docking Configuration

IV. Transfer Trajectories

Transfer of MADD from shuttle to MSS is divided into two phases. Phase one is idealized as having one applied impulse chosen so that the vehicle has appropriate position and velocity components at the rendezvous point. During phase two MADD paces the docking port while closing into dock. Thrust computations are performed in a moving coordinate frame with the origin at the CM of the MSS as illustrated in Figure 3. The X-axis is along the direction of motion, Y-axis is normal to the orbital plane, and Z-axis is along the local vertical. Equations of motion for a transfer trajectory to an object in a nearly circular oribt are well-known.[5] In the moving X,Y,Z frame during phase one, these equations are

$$\begin{aligned} \ddot{x} + 2n\dot{z} &= 0 \\ \ddot{y} + n^2 y &= 0 \\ \ddot{z} - 2n\dot{x} - 3n^2 z &= 0 \end{aligned} \tag{1}$$

where $n = (GM_E/a^3)^{1/2}$, the mean motion of the MSS in its orbit. The solution of set (1) is readily obtained in closed form:

$$\begin{aligned} x(t) &= \frac{2\dot{z}_o}{n} \cos nt + \left(\frac{4\dot{x}_o}{n} + 6z_o\right) \sin nt + \left(x_o - \frac{2\dot{z}_o}{n}\right) - \left(3\dot{x}_o + 6nz_o\right)t \\ y(t) &= y_o \cos nt + \frac{\dot{y}_o}{n} \sin nt \\ z(t) &= \frac{\dot{z}_o}{n} \sin nt - \left(\frac{2\dot{x}_o}{n} + 3z_o\right) \cos nt + \left(\frac{2\dot{x}_o}{n} + 4z_o\right) \end{aligned} \tag{2}$$

With initial conditions

$$x(0) = x_o, \quad y(0) = z(0) = 0$$

set (2) becomes

$$x(t) = \frac{2\dot{z}_o}{n} \cos nt + \frac{4\dot{x}_o}{n} \sin nt + (x_o - \frac{2\dot{z}_o}{n}) - 3\dot{x}_o t$$

$$y(t) = \frac{\dot{y}_o}{n} \sin nt \qquad (3)$$

$$z(t) = \frac{\dot{z}_o}{n} \sin nt - \frac{2\dot{x}_o}{n} \cos nt + \frac{2\dot{x}_o}{n}$$

Initial conditions are based on the assumption that the shuttle is in the orbital plane of the MSS. The out-of-plane Y-component results in simple harmonic motion, while in-plane transfer motion is coupled. The only acceptable values of initial conditions x_o, $\dot{x}_o$, $\dot{y}_o$, and $\dot{z}_o$ are those which result in x, y, z and $\dot{x}$, $\dot{y}$, $\dot{z}$ simultaneously approaching the values x_1, y_1, z_1 and $\dot{x}_1$, $\dot{y}_1$, $\dot{z}_1$, respectively at time $t = t_1$, (rendezvous point). The initial velocity components are given as

$$\dot{x}_o = \frac{n(x_1 - x_o) \sin nt_1 + 2nz_1(1 - \cos nt_1)}{8(1 - \cos nt_1) - 3nt_1 \sin nt_1}$$

$$\dot{y}_o = \frac{ny_1}{\sin nt_1} \qquad (4)$$

$$\dot{z}_o = \frac{nz_1(4 \sin nt_1 - 3nt_1) - 2n(x_1 - x_o)(1 - \cos nt_1)}{8(1 - \cos nt_1) - 3nt_1 \sin nt_1}$$

These resulting expressions indicate that the initial relative velocity requirements for transfer to the rendezvous point are functions of x_o, x_1, y_1, z_1, and time of transfer, t_1. x_o is dependent upon safety of the shuttle to prevent a hazardous situation, and x_1, y_1, z_1 are dependent

upon the location of the docking port at time $t = t_1$. The velocity components are given as

$$\begin{aligned}
\dot{x}(t) &= -2\dot{z}_o \sin nt + 4\dot{x}_o \cos nt - 3\dot{x}_o \\
\dot{y}(t) &= \dot{y}_o \cos nt \\
\dot{z}(t) &= \dot{z}_o \cos nt + 2\dot{x}_o \sin nt
\end{aligned} \tag{5}$$

At time t_1 the velocity components of MADD should be equal to the velocity that point x_1, y_1, z_1 would have if it were fixed to the MSS. Therefore, the velocity components at time t_1 are[6]

$$\begin{aligned}
\dot{x}_1 &= \omega_y z_1 - \omega_z y_1 = -2\dot{z}_o \sin nt_1 + 4\dot{x}_o \cos nt_1 - 3\dot{x}_o \\
\dot{y}_1 &= \omega_z x_1 - \omega_x z_1 = \dot{y}_o \cos nt_1 \\
\dot{z}_1 &= \omega_x y_1 - \omega_y x_1 = \dot{z}_c \cos nt_1 + 2\dot{x}_o \sin nt_1
\end{aligned} \tag{6}$$

From these previous expressions, time t_1 and initial velocity requirements may be determined. ω_x, ω_y, ω_z, y_1 and z_1 are relative to the moving coordinate frame. They are related to the body fixed coordinate frame of the MSS by the following expressions.[6]

$$\begin{bmatrix} x_1 \\ y_1 \\ z_1 \end{bmatrix} = \underline{T(t)} \begin{bmatrix} x_{b1} \\ y_{b1} \\ z_{b1} \end{bmatrix}, \quad t = t_1 \tag{7}$$

$$\begin{bmatrix} \omega_x \\ \omega_y \\ \omega_z \end{bmatrix} = \underline{T(t)} \begin{bmatrix} \omega_{bx} \\ \omega_{by} \\ \omega_{bz} \end{bmatrix}, \quad t = t_1 \tag{8}$$

where

$$\underline{T(t)} = \left[\begin{array}{ccc|ccc|ccc} C\phi_b\, C\psi_b - S\phi_b\, S\psi_b\, C\theta_b & & & -S\phi_b\, C\psi_b - C\phi_b\, S\psi_b\, C\theta_b & & & S\theta_b\, S\psi_b & & \\ C\phi_b\, S\psi_b - S\phi_b\, C\psi_b\, C\theta_b & & & -S\phi_b\, S\psi_b + C\phi_b\, C\psi_b\, C\theta_b & & & -S\theta_b\, C\psi_b & & \\ S\theta_b\, S\phi_b & & & S\theta_b\, C\phi_b & & & C\theta_b & & \end{array}\right] \tag{9}$$

using $C\phi_b = \cos\phi_b$, $S\phi_b = \sin\phi_b$, etc.

Automatic position control during phase two can be modeled by using the nonhomogeneous form of equations (1).

$$\begin{aligned} \ddot{x} + 2nx &= f_x \\ \ddot{y} + n^2 y &= f_y \\ \ddot{z} - 2nx - 3n^2 z &= f_z \end{aligned} \tag{10}$$

where f_x f_y, f_z are the applied acceleration components which are the control and disturbance forces. Initial conditions associated with set (10) become

$$x(0) = x_1, \quad y(0) = y_1, \quad z(0) = z_1$$

$$\dot{x}(0) = \dot{x}_1, \quad \dot{y}(0) = \dot{y}_1, \quad \dot{z}(0) = \dot{z}_1$$

Taking the Laplace transform of the differential equations and solving for X(s), Y(s), and Z(s) gives

$$X(s) = \frac{1}{s} x_1 - \frac{6n^3}{s^2(s^2 + n^2)} z_1 + \frac{s^2 - 3n^2}{s^2(s^2 + n^2)} \dot{x}_1 - \frac{2n}{s(s^2 + n^2)} \dot{z}_1$$

$$+\frac{s^2 - 3n^2}{s(s^2 + n^2)} F_x(s) - \frac{2n}{s(s^2 + n^2)} F_z(s)$$

$$Y(s) = \frac{sy_1 + \dot{y}_1}{s^2 + n^2} + \frac{1}{s^2 + n^2} F_y(s) \tag{11}$$

$$Z(s) = \frac{1}{s^2 + n^2} \dot{z}_1 + \frac{s^2 + 4n^2}{s(s^2 + n^2)} z_1 + \frac{2n}{s(s^2 + n^2)} \dot{x}_1$$

$$\frac{1}{s^2 + n^2} F_z(s) + \frac{2n}{s(s^2 + n^2)} F_x(s)$$

The control law developed is of the form

$$f_{cx} = -K_x(\dot{x} - K_1 x)$$

$$f_{cy} = -K_y(\dot{y} - K_2 y) \tag{12}$$

$$f_{cz} = -K_z(\dot{z} - K_3 z)$$

where x, y, z and $\dot{x}$, $\dot{y}$, $\dot{z}$ are position and velocity errors with respect to the moving coordinate frame. This control law requires position, velocity, and attitude information. It also requires the use of throttleable thrusters or a multifunctional monopropellant propulsion subsystem. The negative signs in the brackets assure negative feedback. Control values, X_c, Y_c, Z_c are computed by the onboard digital computer. Control values f_{c1}, f_{c2}, f_{c3} related to the body fixed coordinate frame of MADD by the following expression:[6]

$$\begin{bmatrix} f_{c1} \\ f_{c2} \\ f_{c3} \end{bmatrix} = \underline{T(t)} \begin{bmatrix} f_{cx} \\ f_{cy} \\ f_{cz} \end{bmatrix} \tag{13}$$

where

$$\underline{T(t)} = \left[\begin{array}{ccc|ccc|cc} C\phi_c\,C\psi_c - S\phi_c\,C\theta_c\,S\psi_c & & & C\phi_c\,S\psi_c + S\phi_c\,C\theta_c\,C\psi_c & & & S\phi_c\,S\theta_c & \\ - S\phi_c\,C\psi_c - C\phi_c\,C\theta_c\,S\psi_c & & & -S\phi_c S\psi_c + C\phi_c\,C\theta_c\,C\psi_c & & & C\phi_c\,S\theta_c & \\ S\theta_c\,S\psi_c & & & - S\theta_c\,C\psi_c & & & C\theta_c & \end{array}\right] \tag{14}$$

using $C\phi_c = \cos\phi_c$, $S\phi_c = \sin\phi_c$ etc.

Figures 5, 6, and 7 illustrate the block diagrams for the three components relative to the moving coordinate frame. The X and Z components are coupled and the Y component is uncoupled. System transfer functions are determined by taking each component separately. The X component has inner loop transfer function.

$$\frac{X}{\varepsilon_1} = \frac{K_x(s^2 - 3n^2)}{s(s^3 + K_x s^2 + n^2 s - 3K_x n^2)}$$

$$GH = \frac{K_x(s^2 - 3n^2)}{s(s^2 + n^2)} \tag{15}$$

and outer loop transfer function

$$\frac{X}{X_c} = \frac{K_x K_1(s^2 - 3n^2)}{s^4 + K_x s^3 + (K_x K_1 + n^2)s^2 - sK_x n^2 s - 3K_x K_1 n^2} \tag{16}$$

$$GH = \frac{K_x K_1(s^2 - 3n^2)}{s(s^3 + K_x s^2 + n^2 s - 3K_x n^2)}$$

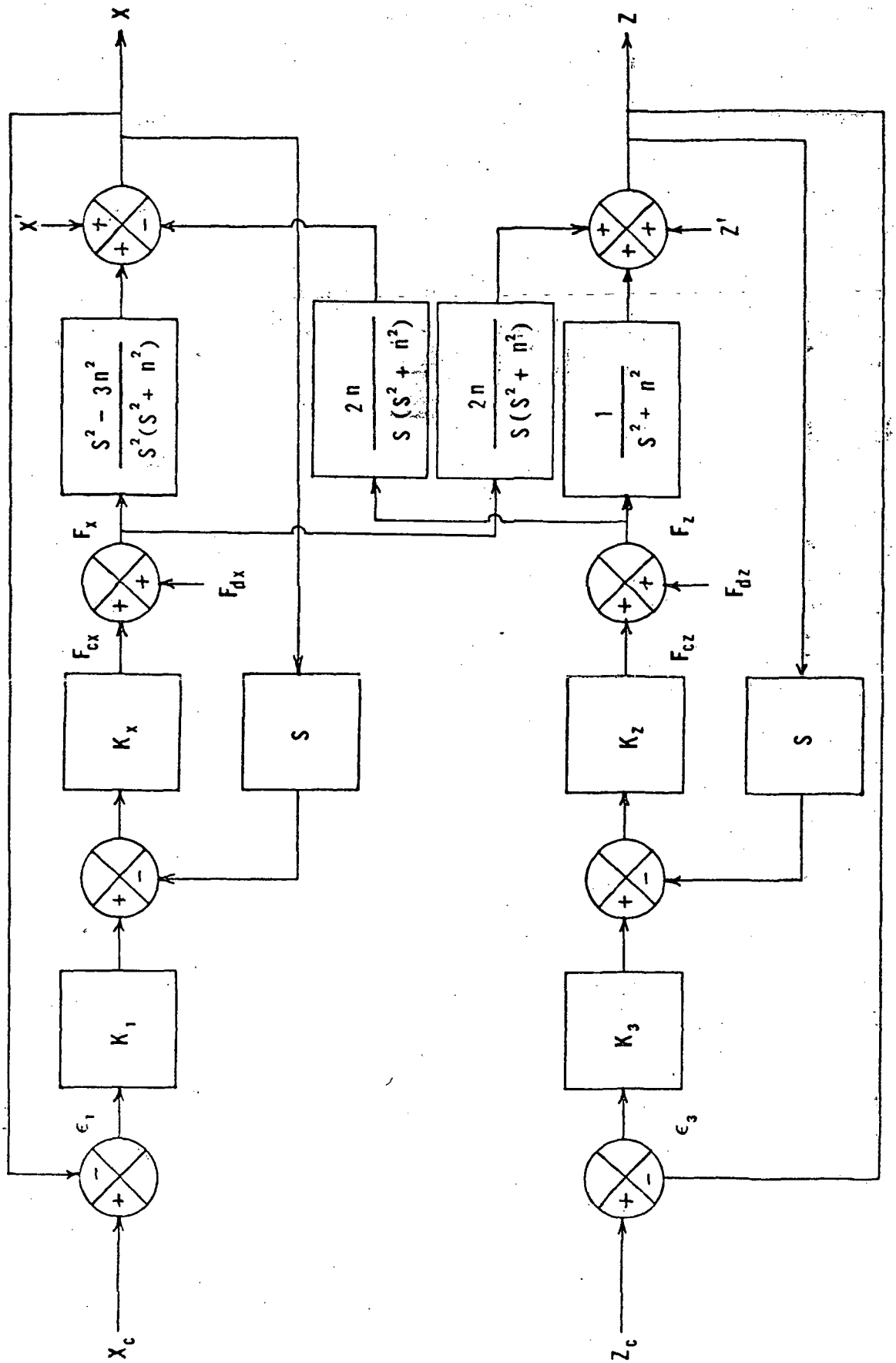

Figure 5. Block Diagram of X and Z Coupled Position Control System

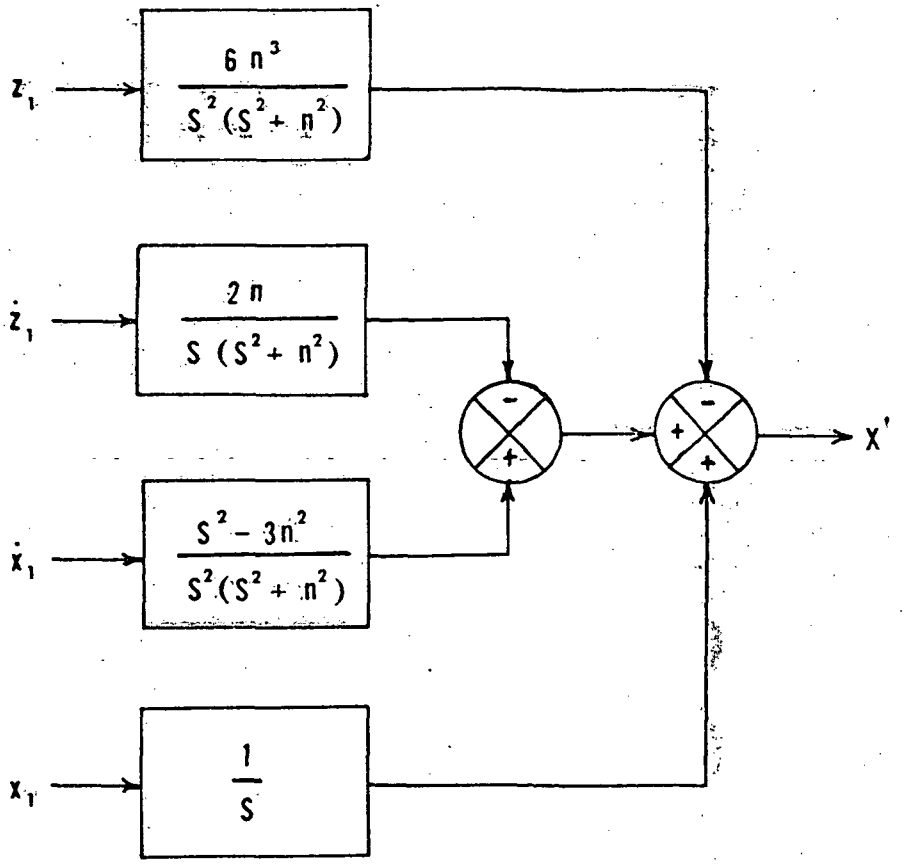

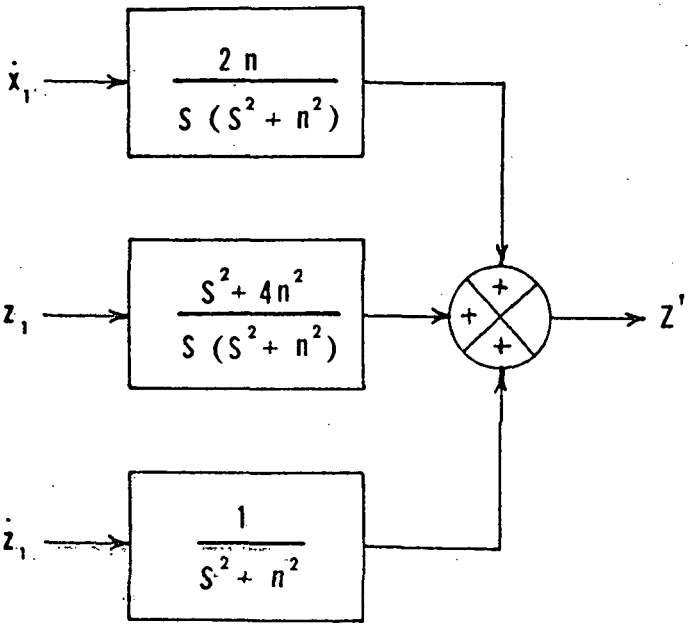

Figure 6. Block Diagram of X and Z Initial Conditions

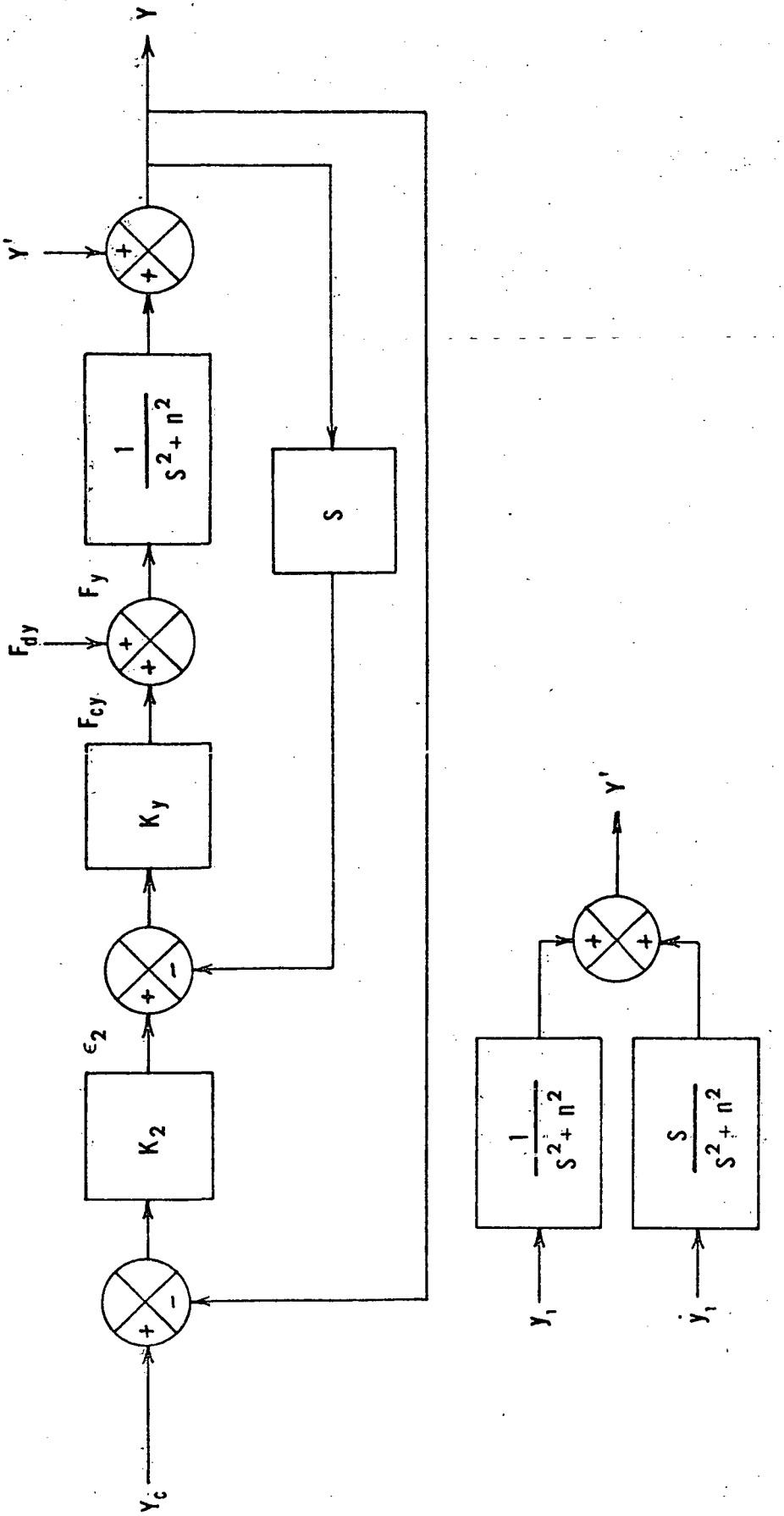

Figure 7. Block Diagram of Y Position Control System

The y component has inner loop transfer function

$$\frac{Y}{\epsilon_2} = \frac{K_y}{s^2 + K_y s + n^2}$$

$$GH = \frac{K_y s}{s^2 + n^2} \qquad (17)$$

and outer loop transfer function

$$\frac{Y}{Y_c} = \frac{K_y K_2}{s^2 + K_y s + (K_y K_2 + n^2)}$$

$$GH = \frac{K_y K_2}{s^2 + K_y s + n^2} \qquad (18)$$

The Z component has inner loop transfer function

$$\frac{Z}{\epsilon_3} = \frac{K_z}{s^2 + K_z s + n^2}$$

$$GH = \frac{K_z s}{s^2 + n^2} \qquad (19)$$

and outer loop transfer function

$$\frac{Z}{Z_c} = \frac{K_z K_3}{s^2 + K_z s + (K_z K_3 + n^2)}$$

$$GH = \frac{K_z K_3}{s^2 + K_z s + n^2} \qquad (20)$$

Steady state errors of the systems for position, velocity, and acceleration were found for each component. For the X control system (class 1 canonical feedback system)

$$e_p(\infty) = \frac{1}{K_p} \lim_{s\to 0} \frac{s(s^3 + K_x s^2 + n^2 s - 3K_x n^2)}{K_x K_1 (s^2 - 3n^2)} = 0$$

$$e_v(\infty) = \frac{1}{K_v} \lim_{s\to 0} \frac{s^3 + K_x s^2 + n^2 s - 3K_x n^2}{K_x K_1 (s^2 - 3n^2)} = \frac{1}{K_1}$$

$$e_a(\infty) = \frac{1}{K_a} = \lim_{s\to 0} \frac{s^3 + K_x s^2 + n^2 s - 3K_x n^2}{K_x K_1 (s^2 - 3n^2)\, S} = \infty$$

For the Y control system (class 0 canonical feedback system)

$$K_p = \lim_{s\to 0} \frac{s^2 + K_y s + n^2}{K_2 K_y} \simeq \frac{n^2}{K_2 K_y}$$

$$e_p(\infty) = \frac{1}{1 + K_p} = \frac{n^2}{n^2 + K_y K_2} \simeq \frac{n^2}{K_y K_2} \quad (K_y K_2 >> n^2)$$

$$e_v(\infty) = \frac{1}{K_v} = \lim_{s\to 0} \frac{s^2 + K_y s + n^2}{K_y K_2} = \infty$$

$$e_a(\infty) = \frac{1}{K_a} = \lim_{s\to 0} \frac{s^2 + K_y s + n^2}{K_y K_2 s^2} = \infty$$

For the Z control system (class 0 canonical feedback system)

$$e_p(\infty) = \frac{n^2}{K_z K_3} \quad (K_z K_3 >> n^2)$$

$$e_v(\infty) = \infty$$

$$e_a(\infty) = \infty$$

The gain of the coupling terms for the X and Z components are of the order of the mean motion n, the coupling has relatively little effect on the X and Z systems. Therefore, the coupling term will be neglected temporarily.

The X component function given by equation (11) is complicated by the two zeros in the numerator of the system equation, $(\pm \sqrt{3}n$. Considering the magnitude of the mean motion, an apporximation is made by cancelling the $s^2 - 3n^2$ term with s^2 in the demoninator. These simplications result in three uncoupled second-order component systems.

The root locus technique was used to determine the performance of the component system.[7] Coupling effects and initial conditions were neglected for the stability analysis. Since coupling is so small, stability should be effected little. The inner and outer loop root locus diagrams for the nonsimplified X component systems are shown in Figures 8 and 9, respectively. The inner and outer root locus diagrams for the Y component system are shown in Figures 10 and 11, respectively. The Z component root locus are similar to the Y root locus.

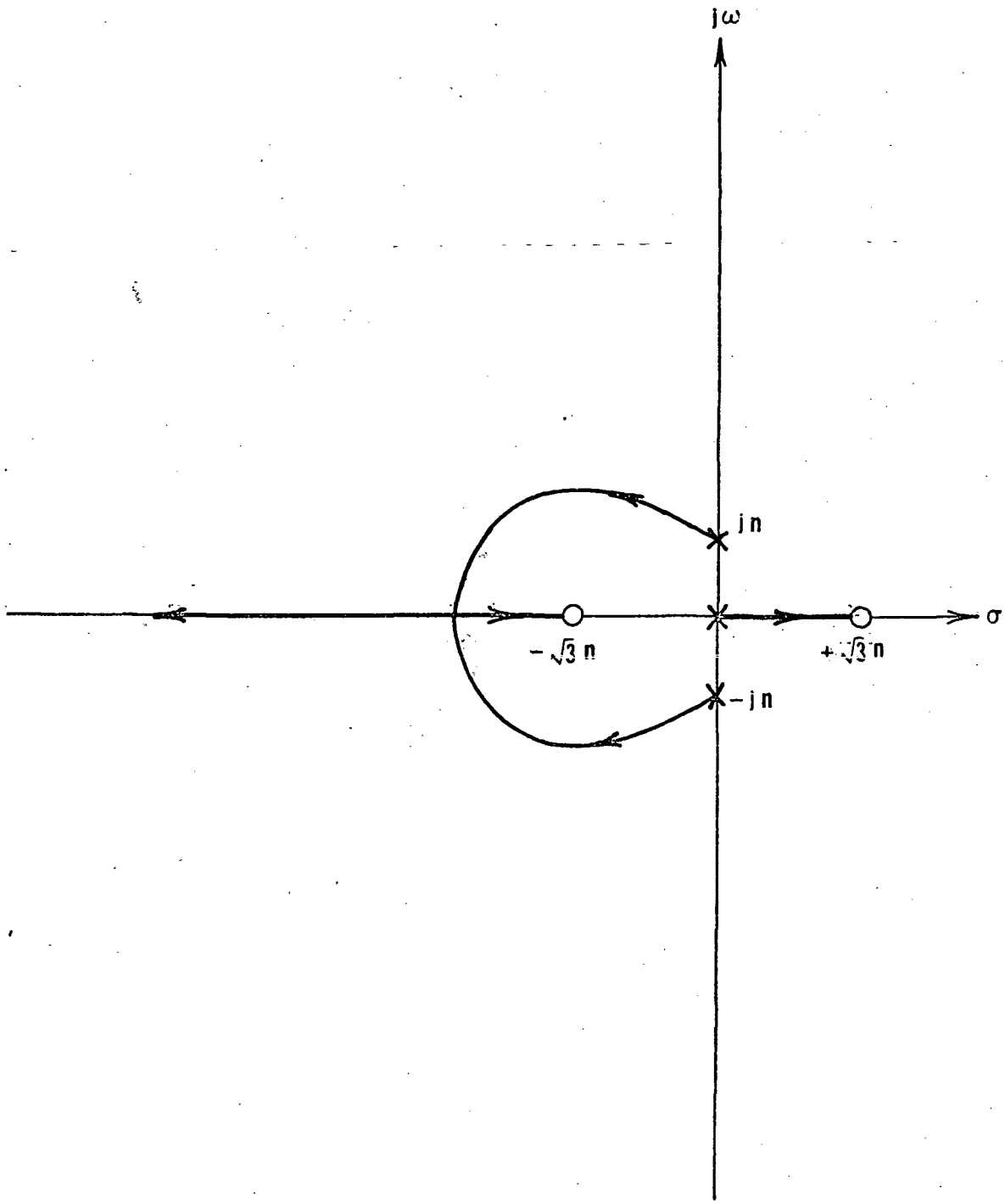

Figure 8. Root Locus Plot for X Component (inner loop)

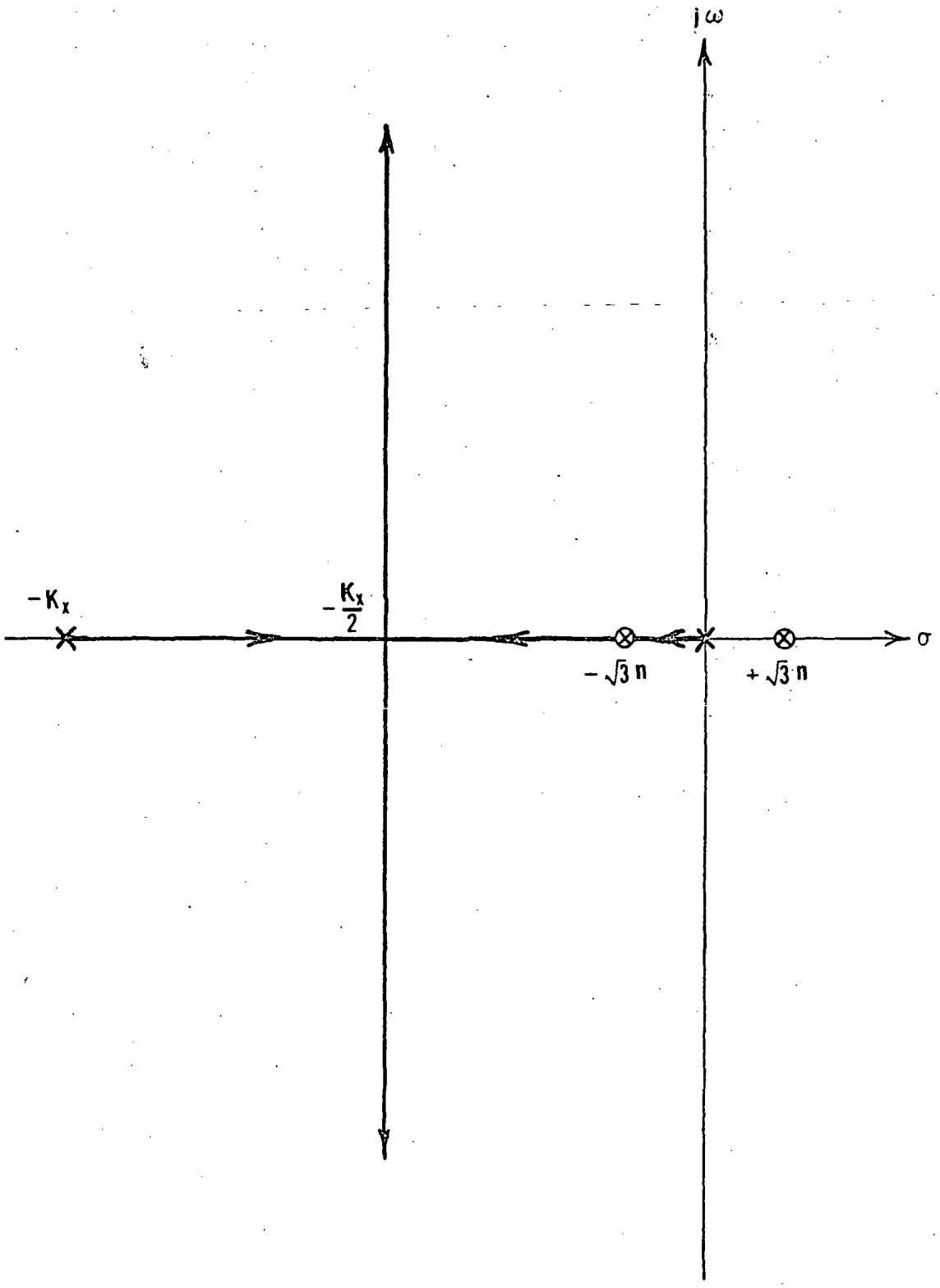

Figure 9. Root Locus Plot for X Component (outer loop)

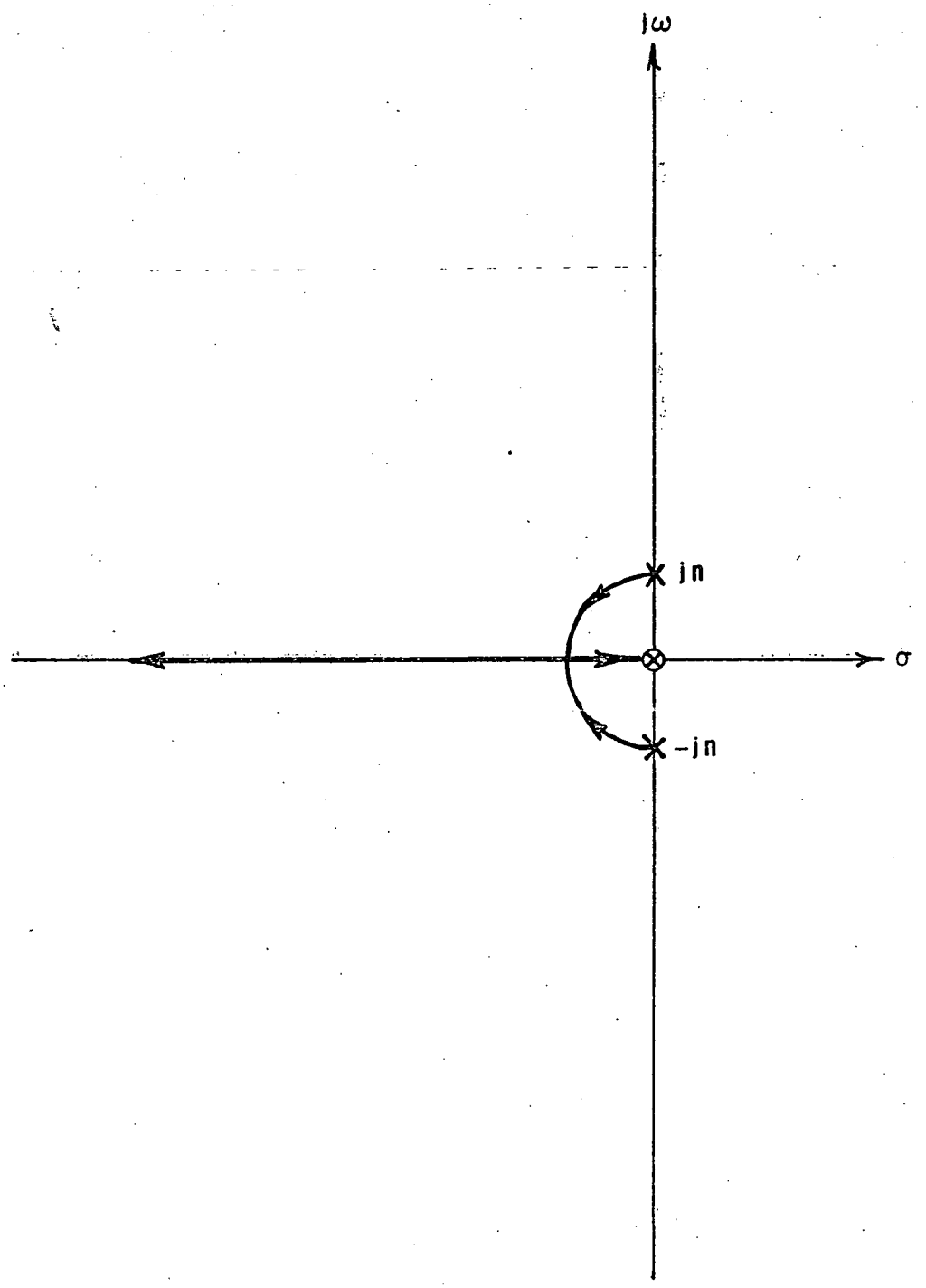

Figure 10. Root Locus Plot for Y and Z Components (inner loop)

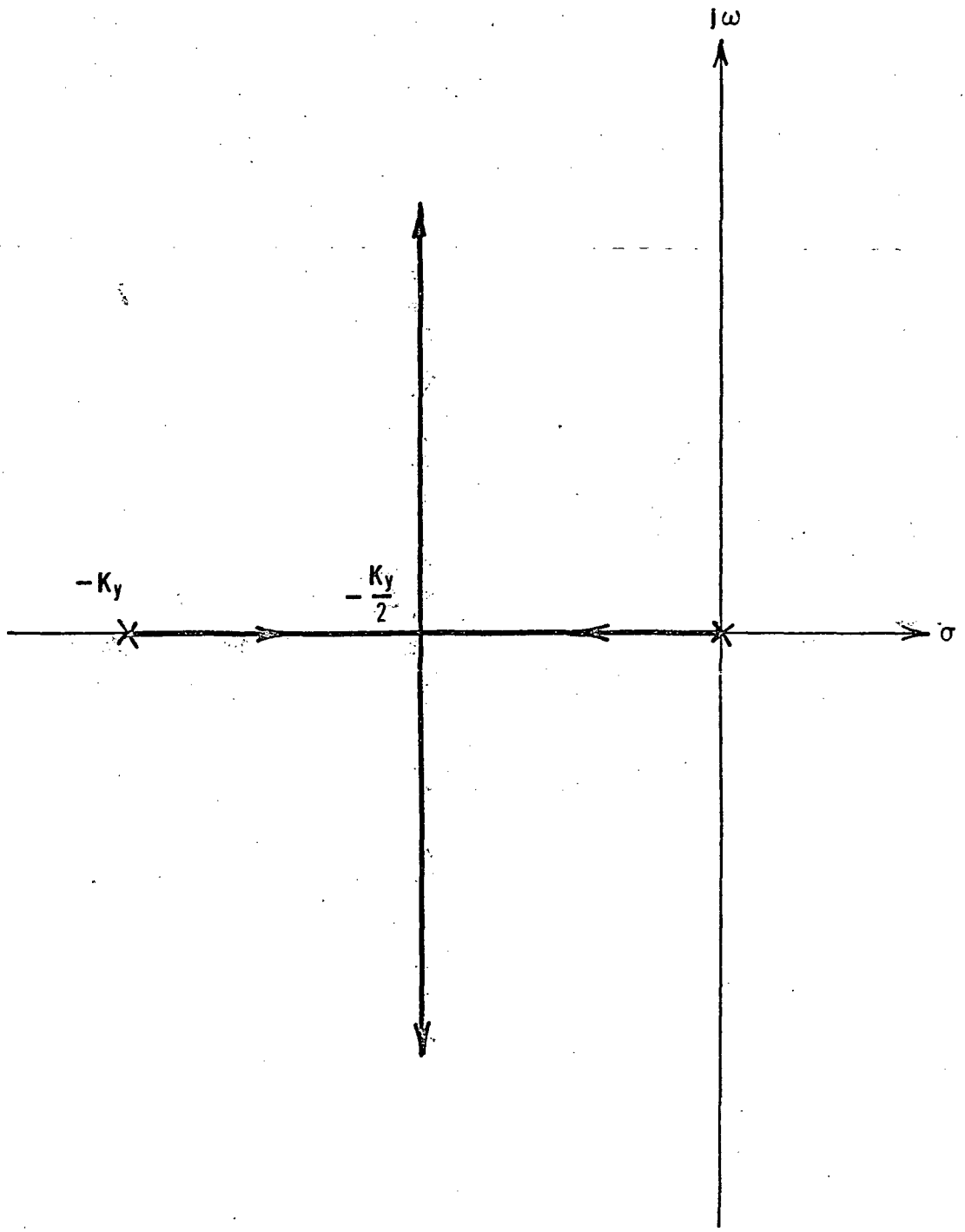

Figure 11. Root Locus Plot for Y and Z Components (outer loop)

Since approximations involving the mean motion and coupling effects between the X and Z components resulted in similar transfer functions, the stability analysis for each system will be similar to that of the Y system. Validity of cancelling the $s^2 - 3n^2$ term with the s^2 on stability of the X component system can be shown qualitatively. The original transfer function has three poles and two zeros in the vicinity of the origin, poles at $\sim K_x/2$, $\pm \sqrt{3n}$, and zero at $\pm \sqrt{3n}$. One zero and one pole ($\pm \sqrt{3n}$) lie in the right-half plane; indicating instability of the system. From the Routh's table the system was found to be unstable for any value of gain. However, the instability is small and will respond long before an instability can reach a significant value.

The root locus for an example control system for the Y - component is shown in Figure 12. The gains K_2 and K_y were chosen to be 100 and 80 respectively and n is given as 1.1×10^{-3} rad/sec. The characteristic equation for a second order system is given by

$$s^2 + 2\zeta\omega_n s + \omega^2_n = s^2 + K_y s + (K_y K_2 + n^2) \qquad (21)$$

Substituting in values of K_2 and K_y, the conditional frequency, ω = 80 rad/sec, the natural frequency, ω_n = 89.5 rad/sec, and the damping ratio, ζ = 0.45. The maximum overshoot for a unit step function input is given by

$$e^{-\pi \zeta/\sqrt{1-\zeta}} = e^{-1.57} = 0.20$$

$$M_p = 1 + 0.20 = 1.20$$

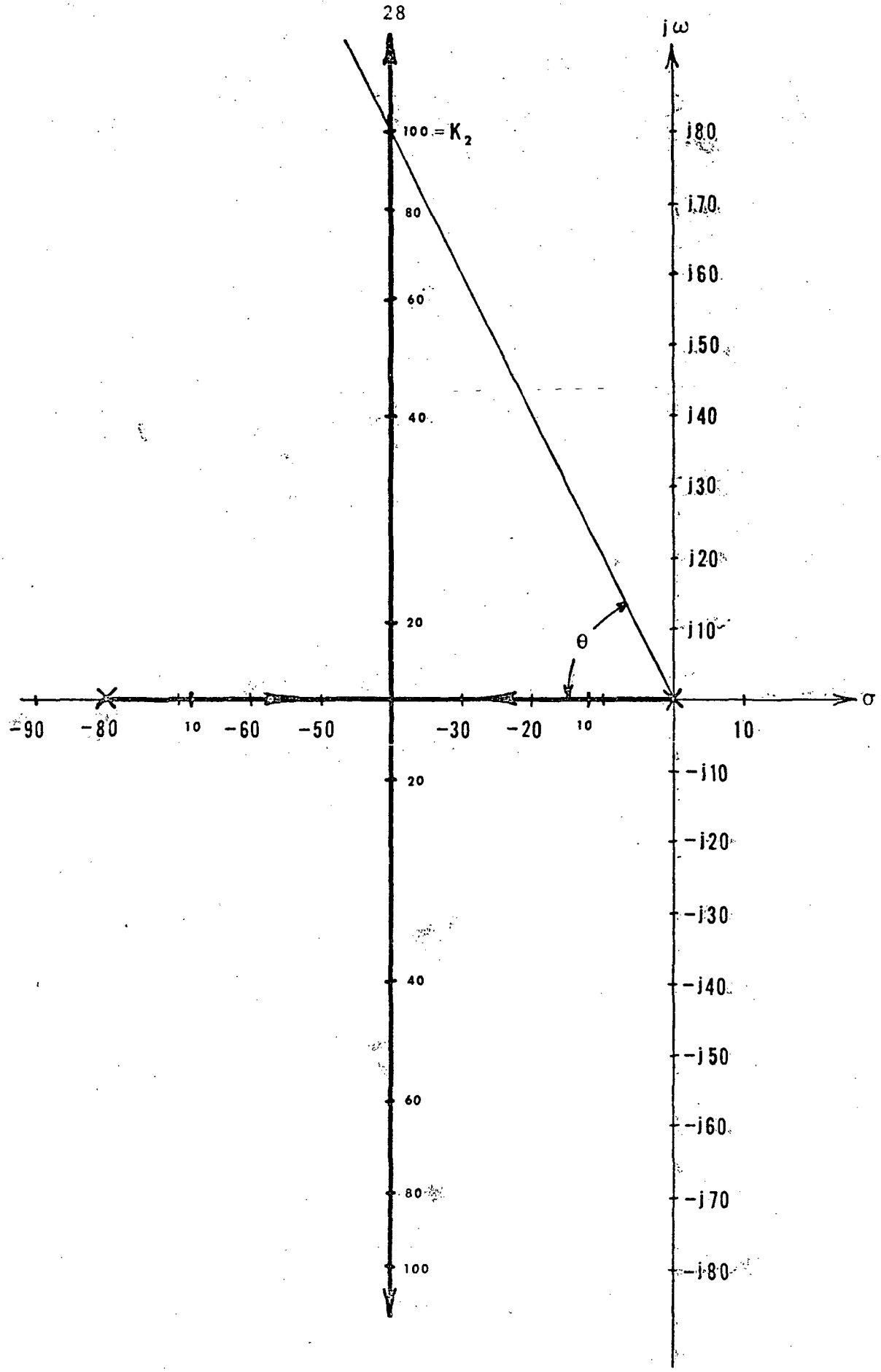

Figure 12. Root Locus Plot for Y Component Position Control System

The rise time is given by the equation[8]

$$T_r = \frac{\omega_{10}t - \omega_{90}t}{\omega_n}$$

$$T_r = \frac{2.0 - 0.4}{89.5} = \frac{1.60}{89.5}$$

$$T_r = 0.018 \text{ sec}$$

A digital simulation of system response was made in order to check the validity of approximations made in the analysis. The digital simulation was simplified by having $f_{dy} = 0$ and initial conditions zero. The resultant block diagram is shown in Figure 13. Gain constants used were the ones used in the previous analysis, $K_y = 80$ and $K_2 = 100$. The Y component system response in position was found for unit step, ramp, and sine inputs. The sine input had a period of 30 sec. (2RPM) and approximates Y_c for a tumbling situation. The response for these inputs are shown in Figure 14. Significance of the mean motion mangitude on response was found to be negligible for these values of gain constants. For a sine input (f = 2 RPM) with magnitude of 18.3 m (60 ft) the error was approximately 3 cm (1.2 in). Thus, the response of the Y-component system represents all three systems.

From these considerations it seems possible to use three simple control systems as illustrated in Figure 7 to maintain the proper position of MADD during phase two of the mission.

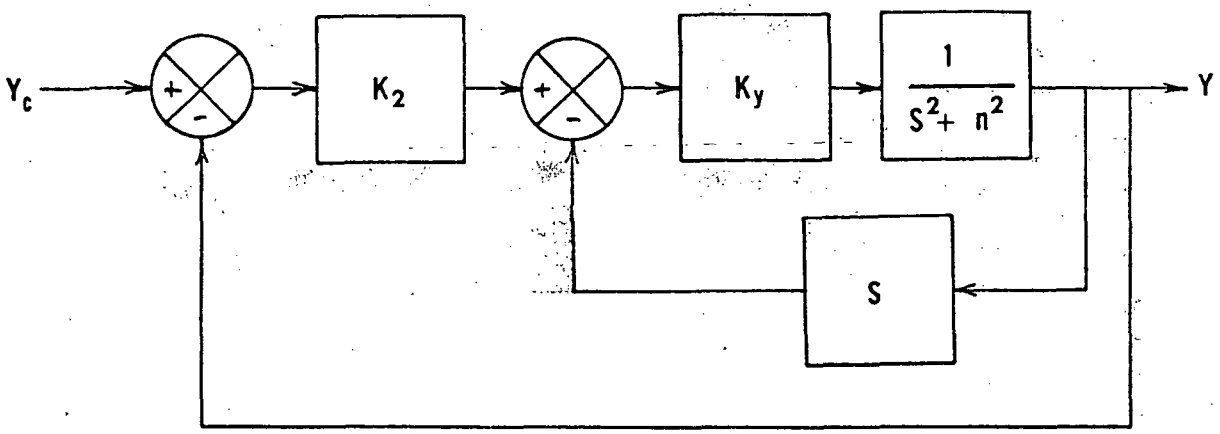

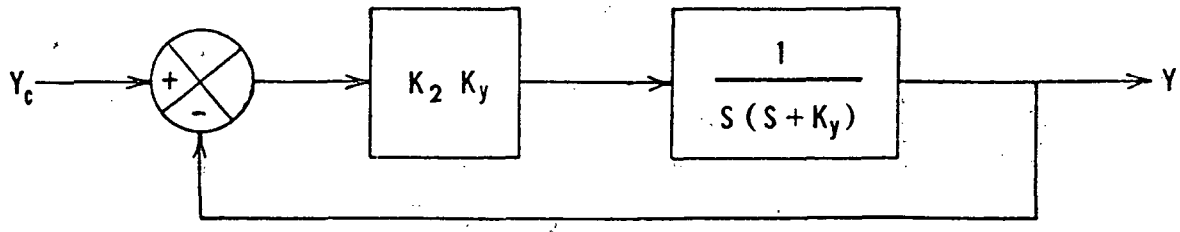

Figure 13. Simplified Y Component Position Control System

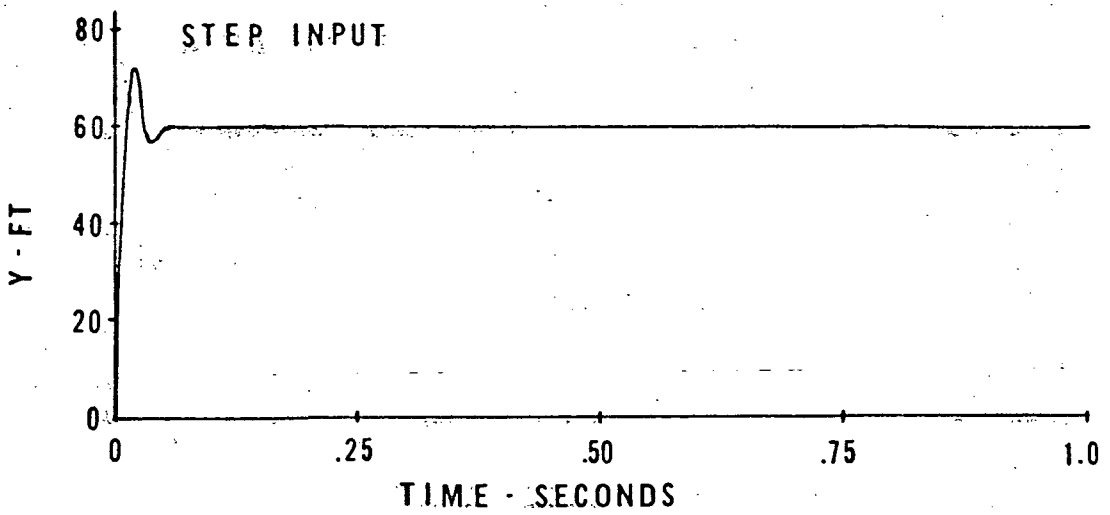

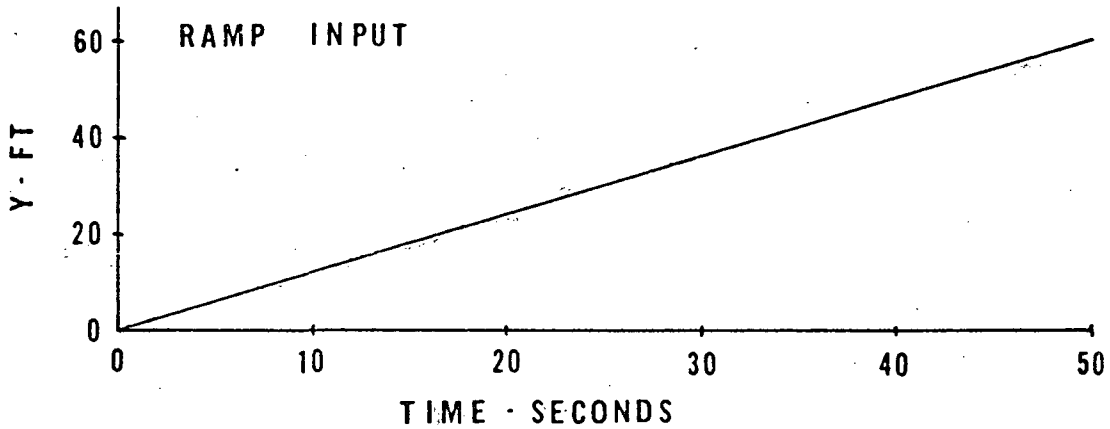

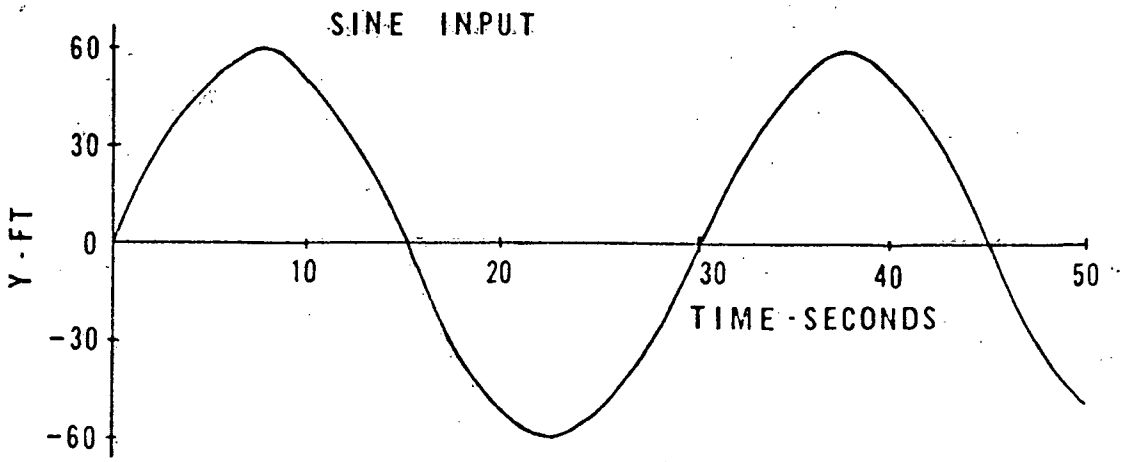

Figure 14. Responses for Simplified Y Component Position Control System

V. Attitude Control Systems

Development of the attitude control systems for MADD are considered in this section. Two attitude control systems are required during the mission: (1) momentum exchange during phase one; and (2) mass explusion during phase two. Attitude control is not required during phase three since MADD is docked with the MSS and being detumbled. MADD stabilization and control systems (SCS) normal modes of operation include: (1) Acquisition establishes the desired three-axis orientation upon deployment of MADD from the shuttle; (2) Reorientation includes the slew and capture of MADD from one known orientation to another with continuous attitude during the maneuvers; and (3) ΔV mode provides the SCS configuration with continuous attitude control during periods of velocity change.

Requirements and constraints on the control systems for MADD include the following areas: (1) sensor type, thruster location, disturbances, MADD configuration; (2) stabilization during velocity - change (ΔV) maneuvers; (3) stabilization and control accuracy and their leverage on system design; (4) attitude rate control; (5) attitude maneuverability; (6) three control degrees of freedom; (7) SCS modes of control; (8) MADD dynamic model; (9) MADD static model; and (10) weight restrictions, power availability, and reliability.

Utilization of software techniques requires accurate dynamic models in the following areas: (1) accurate rigid-body dynamics, including center-of-mass shifts, inertia values, and physical locations; (2) sensor models, including dynamic and stochastic error representations of sensor noise; and (3) torque-producing mechanism dynamics, including nonlinearities and realistic nonrepeatabiltiy models (stochastic parameter variations). This model accuracy is needed for the application of sophisticated onboard data-processing techniques. Because of the very

short duration of the mission elastic-body dynamics and nonstatic physical modeling effects such as thermal deformation are small and will not be needed in the dynamic model of MADD.

Twin gyro controllers and thrusters are used for attitude control. Twin gyro controllers are used for phase one and have the following advantages: (1) first order cross-coupling terms are eliminated by using two-counter-rotating gyros; (2) less power and weight are required for a given momentum exchange capability; and (3) larger gimbal angles may be used so that a major portion of the stored momentum can be transferred to MADD. The equations of motion for a twin gyro controller are[9]

$$\begin{aligned} I_x\dot{p} &= -2\,C_z\Omega_z\,\dot{\delta}_z + L_x \\ I_y\dot{q} &= -2\,C_x\Omega_x\,\dot{\delta}_x + L_y \\ I_z\dot{r} &= -2\,C_y\Omega_y\,\dot{\delta}_y + L_z \end{aligned} \tag{22}$$

The small perturbation approach was used to uncouple the equations, thus, the second order terms can be neglected. From the equations, it is apparent that the controller on the X-axis controls the Y-axis, Y controls Z, and Z controls X, respectively. By using identical gyros on all three axes.

$$C = C_x = C_y = C_z \quad \text{and} \quad \Omega = \Omega_x = \Omega_y = \Omega_z$$

Therefore, the control equations for each axis are the same except for the moment of inertia about that axis. The three axes can be controlled

by an identical control system except for the system gain which would vary with the moments of inertia. A block diagram for the yaw rate system is shown in Figure 15[9]. The root-locus of this control system is shown in Figure 16.

Attitude control for phase two is accomplished by using thrusters placed about the control axes. Mass-expulsion devices are generally inefficient as compared to momentum-exchange devices. Thrusters were chosen because the spin vector in not inertially oriented, and momentum-exchange devices are incapable of continuously reorienting the spin vector without continuous momentum dumping. The attitude control system must allow the simultaneous rotation about all three body axes of MADD. The control law is symthesized from Euler's theorem on rotation which states that any attitude change of a rigid body may be accomplished by a single rotation about a properly chosen axis. This axis of rotation is the eigenvector of the direction cosine matrix defining the orientation of MADD's present position with respect to the command position.

A control law must be specified that will drive the present attitude of MADD, given by a 3 x 3 direction cosine matrix defined as $\underline{A}_{as}$ to the command attitude, given by a 3 x 3 direction cosine matrix defined as $\underline{A}_{cs}$ in a continuous manner.

Orientation of MADD and command orientation are expressed in terms of the moving coordinate system by

$$\begin{bmatrix} \bar{a}_1 \\ \bar{a}_2 \\ \bar{a}_3 \end{bmatrix} = \underline{A}_{as} \begin{bmatrix} \bar{s}_1 \\ \bar{s}_2 \\ \bar{s}_2 \end{bmatrix} \begin{bmatrix} \bar{c}_1 \\ \bar{c}_2 \\ \bar{c}_3 \end{bmatrix} = \underline{A}_{cs} \begin{bmatrix} \bar{s}_1 \\ \bar{s}_2 \\ \bar{s}_3 \end{bmatrix} \tag{23}$$

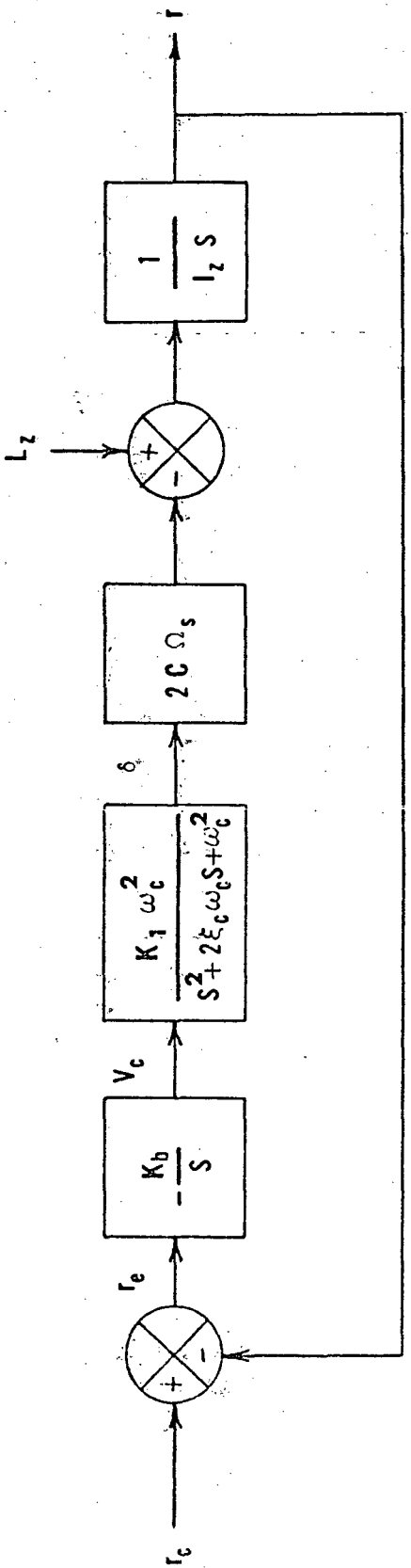

$$K_1 = \frac{K_c I_z}{4C^2\Omega^2 + I_z K_c K_g}$$

$$\omega_c^2 = \frac{4C^2\Omega^2 + I_z K_c K_g}{2I_z(I_a + A)}$$

$$\xi_c = \frac{K_f}{4\omega_c(I_a + A)}$$

Figure 15. Yaw Rate Control System

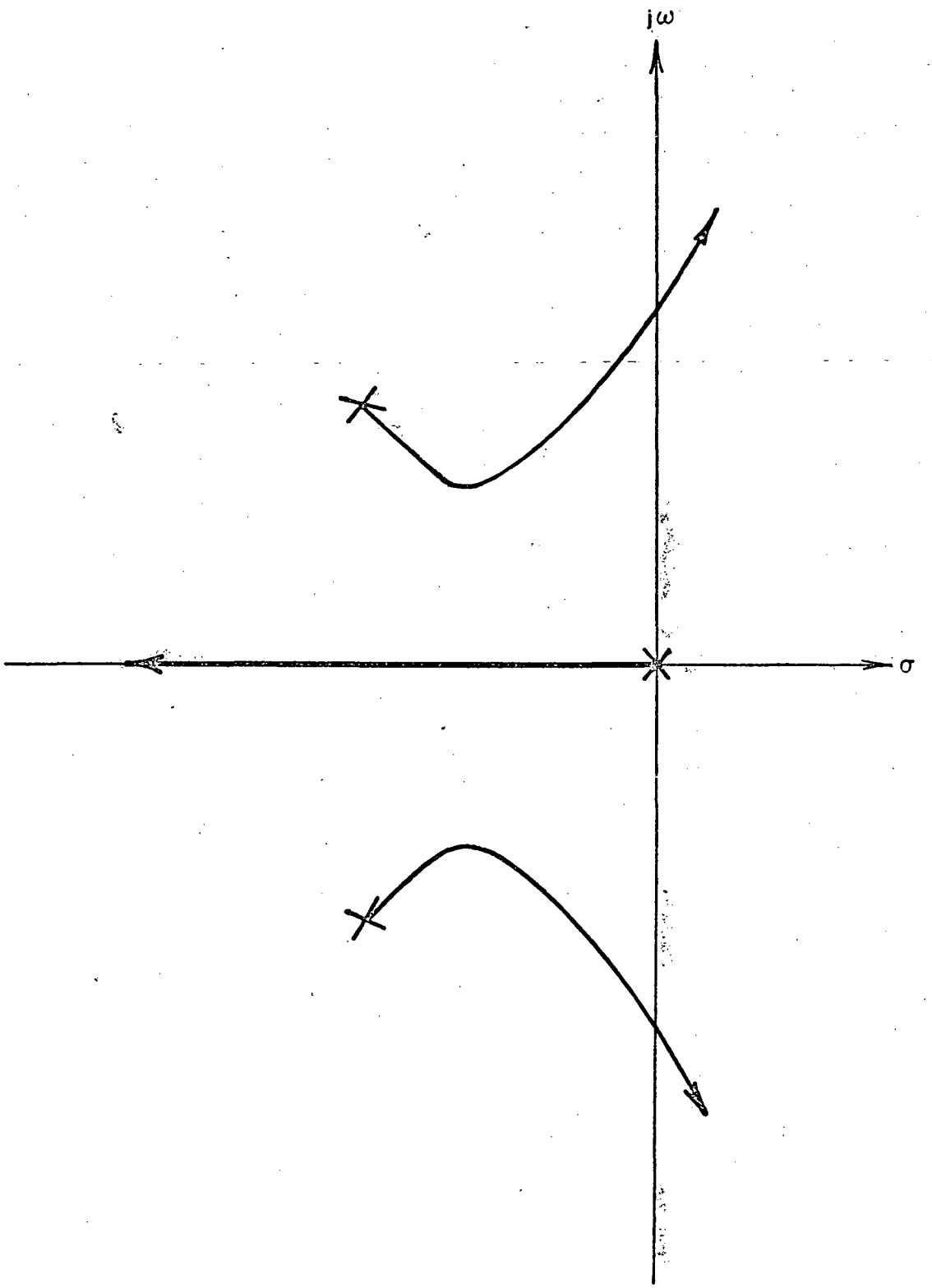

Figure 16. Root Locus Plot for Yaw Rate Control System

Since $\underline{A}_{cs}$ is an orthogonal matrix ($\underline{A}_{cs}^{-1} = \underline{A}_{cs}^{T}$) and from equation 14 the orientation of MADD with respect to the command orientation is given by

$$\begin{bmatrix} \bar{a}_1 \\ \bar{a}_2 \\ \bar{a}_3 \end{bmatrix} = \underline{A}_{as}\ \underline{A}_{cs}^{T} \begin{bmatrix} \bar{c}_1 \\ \bar{c}_2 \\ \bar{c}_3 \end{bmatrix} \qquad (24)$$

MADD will attain the command attitude when the matrix product $\underline{A}_{as}\ \underline{A}_{cs}^{T}$ forms an identity matrix. The matrix product $\underline{A}_{as}\ \underline{A}_{cs}^{T} = \underline{E}$ is defined as the error matrix. Control law information will be extracted from this matrix.

The elements of $\underline{A}_{as}$ will be measured by an onboard inertial platform and are given by the following matrix

$$\underline{A}_{as} = \left[\begin{array}{ccc|c|c} C\phi_a\, C\psi_a - S\phi_a\, C\theta_a\, S\psi_a & & & C\phi_a\, S\psi_a + S\phi_a\, C\theta_a & S\phi_a\, S\theta_a \\ -S\phi_a\, C\psi_a - C\phi_a\, C\theta_a\, S\psi_a & & & -S\phi_a\, S\psi_a + C\phi_a\, C\theta_a & C\phi_a\, S\theta_a \\ S\theta_a\, S\psi_a & & & -S\theta_a\, C\psi_a & C\theta_a \end{array}\right] \qquad (25)$$

using $C\phi_a = \cos\phi_a$, $S\phi_a = \sin\phi_a$, etc.

Where ψ_a, ϕ_a, and θ_a are the measured Euler angles of MADD with respect to the moving frame. The geometry of the coordinate frames relative to the moving frame are shown in Figure 17. The coordinate frame of MADD is translated in the Z direction and the X and Y axes remain parallel to those of the docking reference. The docking reference frame is translated relative to the body fixed axes of the MSS and is fixed. With these conditions, proper orientation of MADD will occur when Euler angles and rates are equal to those of the body fixed frame relative to the moving coordinate frame. Since all the elements

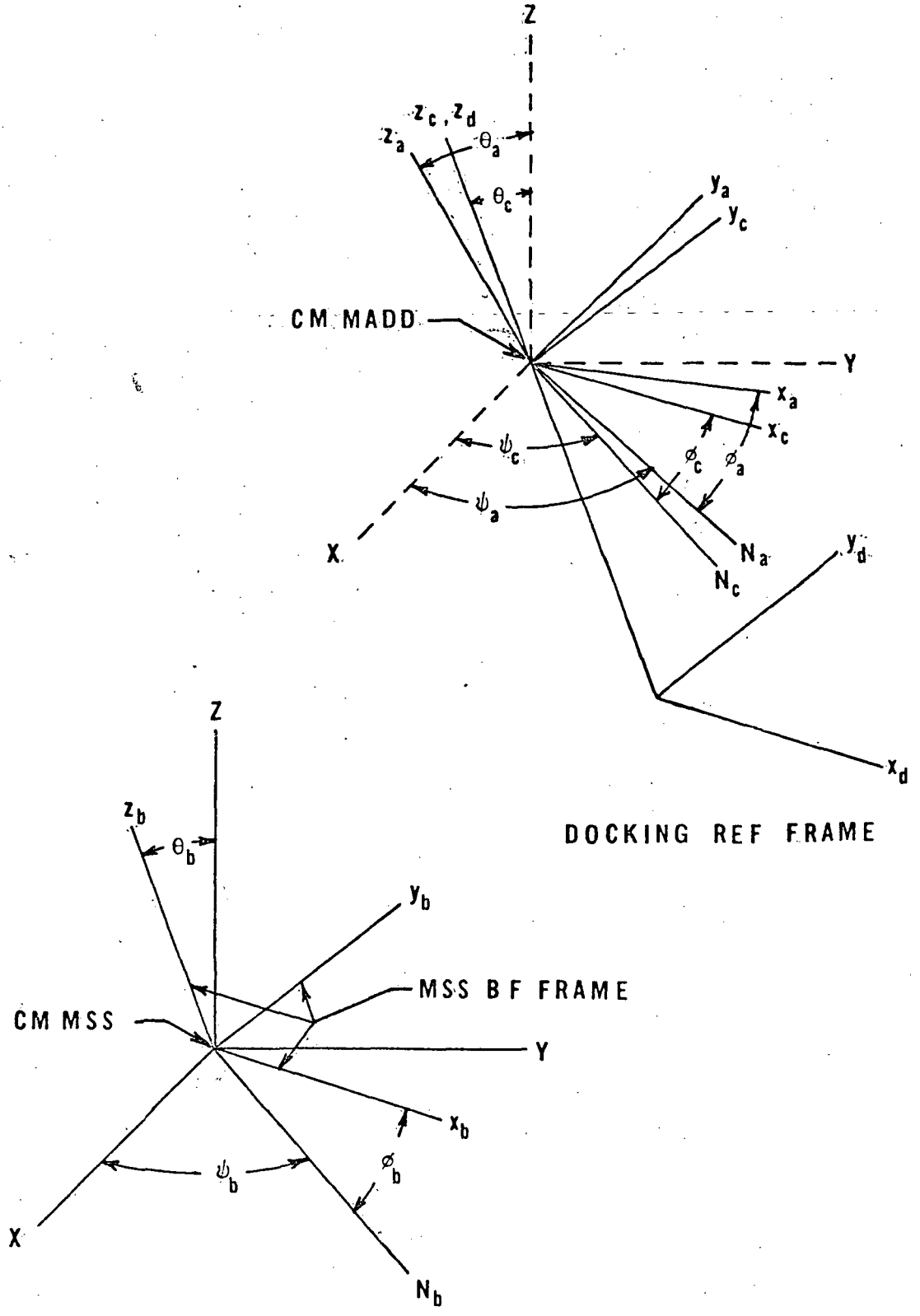

Figure 17. Coordinate Frames Used During Rendezvous and Docking

of $\underline{A}_{as}$ are known and the elements of $\underline{A}_{cs}$ can be computed because of the previous restrictions, the error matrix $\underline{E}$ can be computed from Equation 24.

According to Euler's theorem on rotation, the eigenvectors of the $\underline{E}$ matrix b, is the axis about which MADD is rotated to obtain the command orientation. The angle of rotation about this axis is β. The control law is developed such that control torques to the torques L_x, L_y, and L_z do not exceed design values but the system response must be fast. The control law developed is of the form[10]

$$L_i = - \frac{I_i \, L(max)}{I(max)} \quad [SAT(\beta, \beta_s) \, b_i + \frac{\omega_{ai}}{\omega_a(max)}] \tag{26}$$

$$(i = x,y,z)$$

$L(max)$, $I(max)$, $\omega_a(max)$ are the maximum values of control torques, moments of inertia, and body rate respectively. Ther term $SAT(\beta, \beta_s)$ is a given term derived from the error matrix E:

$$SAT(\beta, \beta_s) = 1 \text{ for } \beta \geq \beta_s$$

$$= \beta/\beta_s \text{ for } \beta < \beta_s \tag{27}$$

The system saturation level is set by this term. Since $L(max)$, $I(max)$, $\omega_a(max)$ are constants for a given rescue mission the control law can be simplified to give

$$L_i = - K_{Ai}[SAT(\beta, \beta_s) + K_B \, \omega_{ai}] \tag{28}$$

$$(i = x,y,z)$$

The terms of b_x, b_y, and b_z are the components of the eigenvector b in the respective body axes and are given by

$$b_x = \frac{1}{2}\left(\frac{E_{23} - E_{32}}{\sin \beta}\right), b_y = \frac{1}{2}\left(\frac{E_{31} - E_{13}}{\sin \beta}\right)$$

$$b_z = \frac{1}{2}\left(\frac{E_{12} - E_{21}}{\sin \beta}\right) \tag{29}$$

where

$$\underline{E} = \begin{bmatrix} E_{11} & E_{12} & E_{13} \\ E_{21} & E_{22} & E_{23} \\ E_{31} & E_{32} & E_{33} \end{bmatrix} \tag{30}$$

Because of disturbance torques and nonsymmetrical mass configuration the components of the eigenvector are time-variant.

The angle β is derived from the $\underline{E}$ matrix and is given by

$$\beta = \cos^{-1}\left[\frac{1}{2}(E_{11} + E_{22} + E_{33} - 1)\right] \tag{31}$$

A block diagram of the attitude control system is shown in Figure 18. The attitude information from the inertial platform and rate gyros is converted from analog form to digital form by the digital computer by an analog to digital converter (ADC). Digital orientation information is processed to form the $\underline{A_{as}}$ matrix. This is multiplied with the command $\underline{A_{cs}}^T$ matrix and the error matrix $\underline{E}$ is generated. The components of the eigenvector $\bar{b}$ and β are computed and body rates are supplied to generate the control law. Control law information is converted from digital to analog form by a digital to analog converter (DAC).

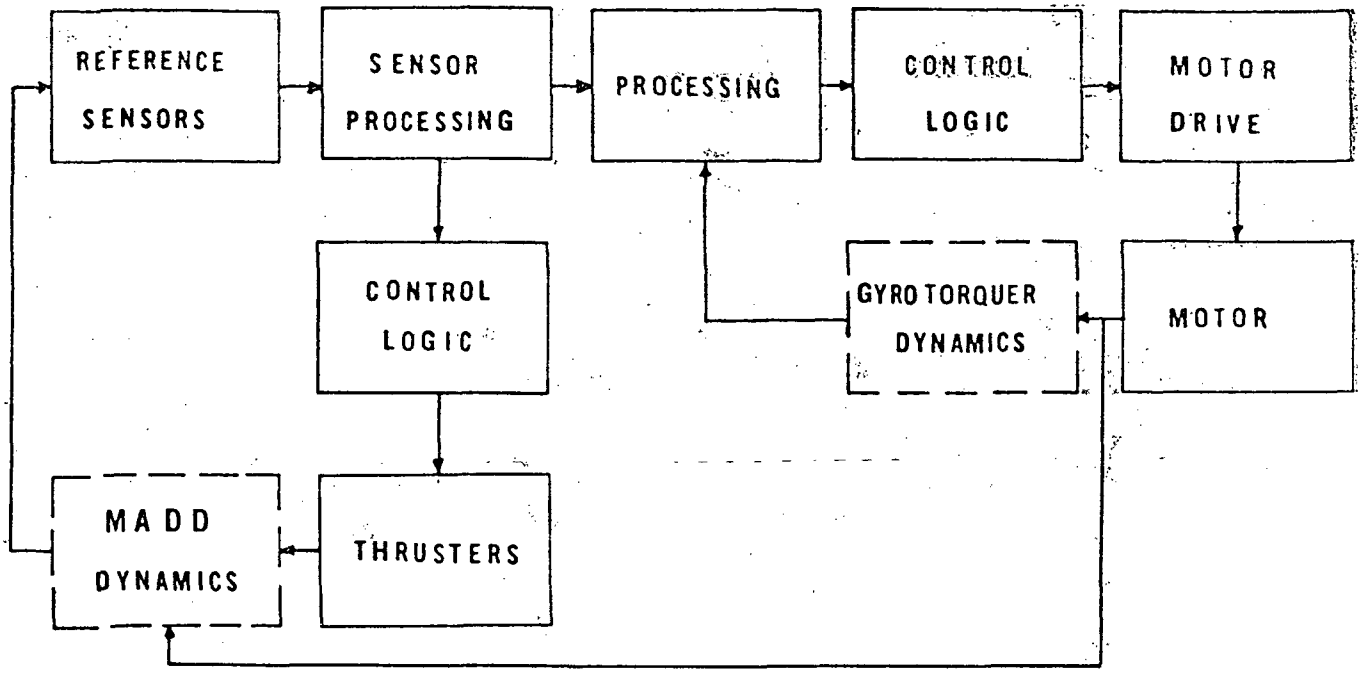

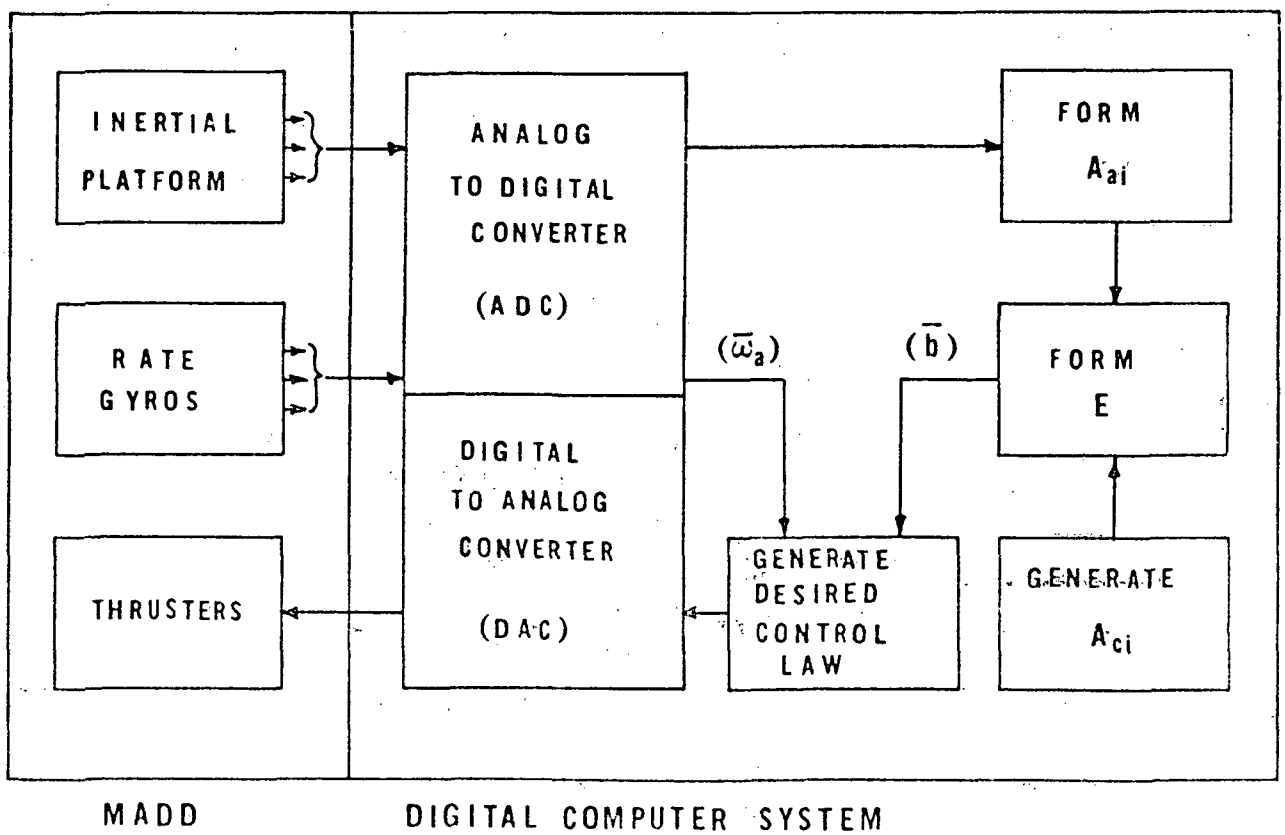

Figure 18. Block Diagram of Attitude Control System

This will provide the thrusters with a continuous thrust profile to orient MADD during phase two of the mission.

A digital simulation of the attitude control system was made to check the accuracy of the control law, (Equation 26), for a given tumbling situation. The command attitude was computed by using the rigid body euler moment equations with zero moment applied to the MSS. The actual attitude and angular rates of MADD were computed by using the rigid body euler moment equations with control moments applied to MADD.

For the simulation the following assumptions were made and initial conditions chosen. For the MSS at t = 0

$$\omega_1 = 0.01 \text{ RPM}, \quad \omega_2 = 0.00 \text{ RPM}, \quad \omega_3 = 1.00 \text{ RPM}$$

$$\psi = 0.0°, \quad \phi = 0.0°, \quad \theta = \theta_L$$

where

$$\theta_L = \sin^{-1} \left[\frac{T^* - I_{13}}{1 - I_{13}} \right]^{1/2}$$

$$I_{13} = \frac{C}{A}, \quad T^* = \frac{T}{T_{max}}, \quad T_{max} = \frac{H^2}{2C}$$

$$T = \frac{1}{2}(A\,\omega_1^2 + B\,\omega_2^2 + C\,\omega_3^2)$$

$$H^2 = A^2\,\omega_1^2 + B^2\,\omega_2^2 + C^2\,\omega_3^2$$

For MADD at t = 0

$$\omega_1 = 0.01 \text{ RPM}, \quad \omega_2 = 0.00 \text{ RPM}, \quad \omega_3 = 1.00 \text{ RPM}$$

$$\psi = 0.10°, \quad \phi = 0.10°, \quad \theta = \theta_L + 0.10°$$

$I_1 = I_2 = 56.2$ Kg-m^2 (1.33×10^3 lbm-ft^2), $I_3 = 423$ Kg-m^2 (1.00×10^4 lbm-ft^2)

$\omega_a(\max) = 1.00$ RPM

$\beta_{s_x} = 10°$

L(max) = (0.1 ft-lb)

The rendezvous point was chosen to be

X = - 2.17m(-7.13 ft), Y = - .915m(-3.00 ft), Z = 24.2m(79.5 ft)

(MSS body fixed frame)

closing rate during docking was 3.04cm/sec(0.1 ft/sec).

The responses of MADD's attitude control system are shown in Figure 19. Part (a) shows that angular rates and part (b) shows the euler angles during phase two of the mission. The actual euler angles had a maximum error of 0.5° relative to the command attitude during closure and the accuracy of the euler angles were found to be controlled by the proper choice of L(max). From this simulation it seems that the control law and technique for applying this control law is capable of maintaining the proper attitude of MADD during phase two of the mission.

The control-torquer assemblies during phase two consist of: 1) propulsion and 2) motors and actuators, etc. MADD attitude-control system requires the capability of a single-propellant supply system to provide precise continuous thrust levels within a given thrust range. Different attitude-control thrust levels are achieved by either a throttleable

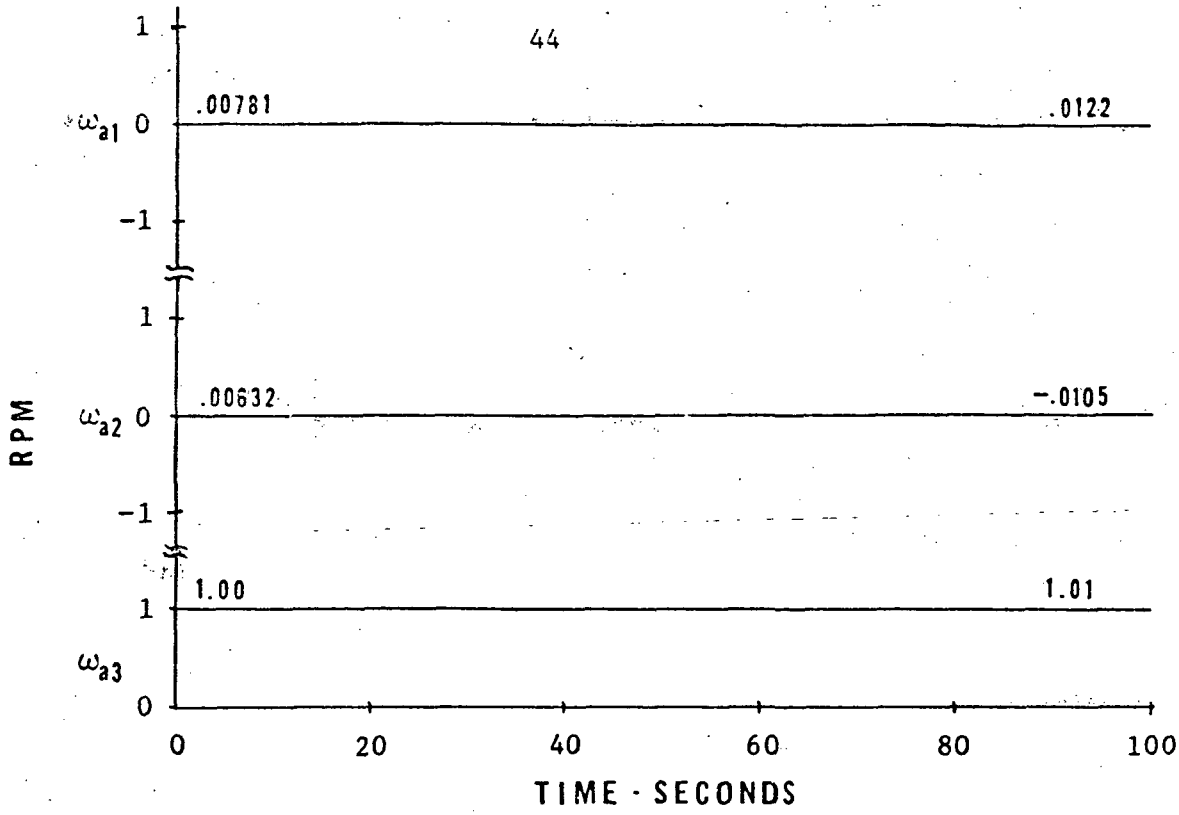

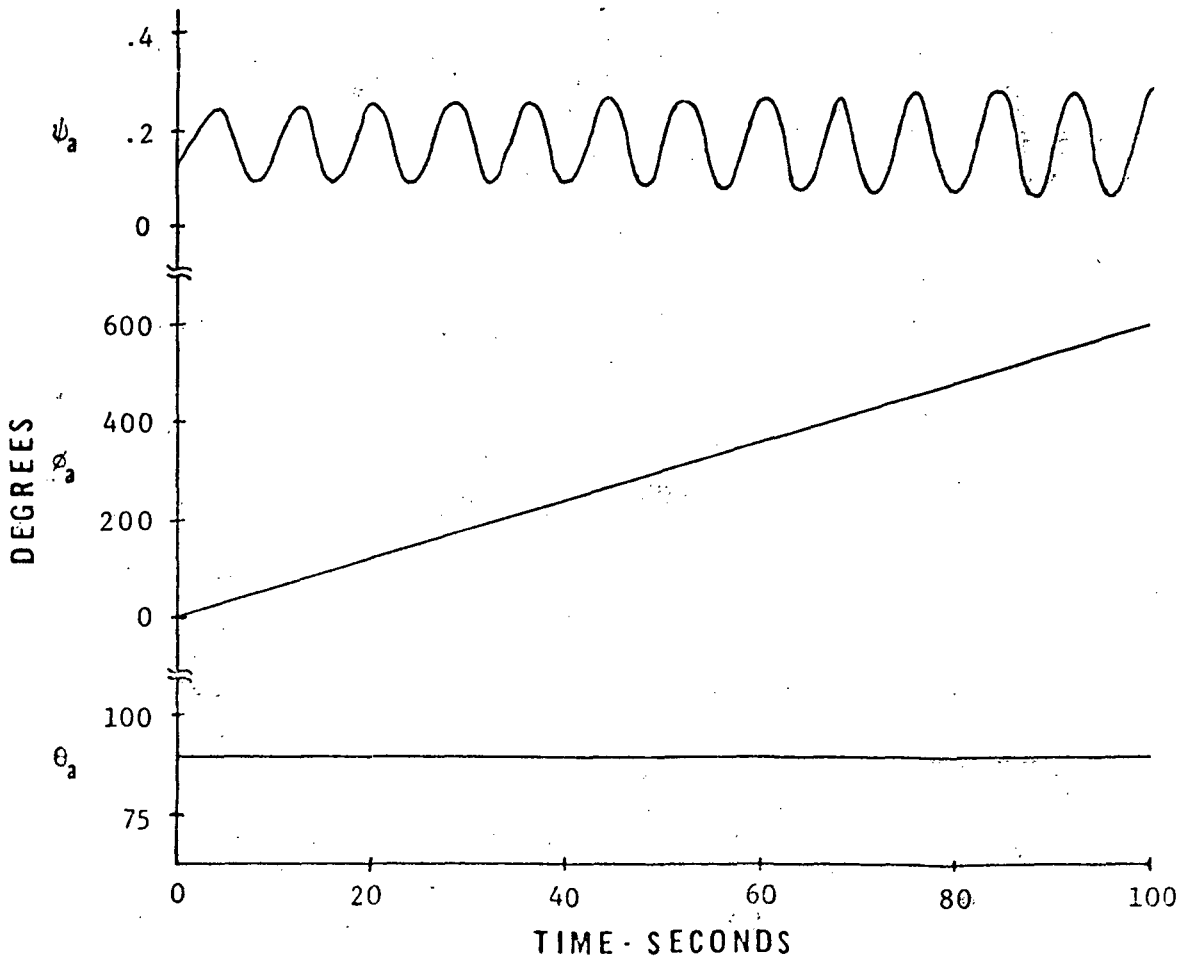

Figure 19. Response of Attitude Control System

thruster or a multifunctional monopropellant propulsion subsystem. The propulsion system will use monopropellant hydrazine for position and attitude control. The throttleable thruster will have one-to-two-orders-of-magnitude thrust variability and the multifunctional monopropellant propulsion subsystem has a four-to-five-orders-of-magnitude thrust variability. The choice between the two schemes will depend upon thrust requirements as well as desired flexibility between different rescue situations.

Backup modes may use different sensors and/or different control schemes than those used to change attitude during operation in the normal mode. The backup modes will exhibit some objectionable characteristics such as reduced performance, degraded reliability, or increased energy expenditure.

The point may be brought up that since the maximum duration of the mission is only a few hours, the need for backup SCS modes may be unnecessary (unwarranted). The reliability of the primary (normal) modes might be high enough to make the backup modes redundant and penalizing MADD with additional weight and space, unnecessary complexity, and increased cost. Tradeoffs maybe made between increased cost of primary with increased reliability without a backup and decreased cost of primary with backup adding to the total cost. The final choice will have to be made depending on the state-of-the-art at the time of the final design of MADD.

The costs of SCS for MADD will be less with the incorporation of general-purpose digital computation, i.e., system standardization. Development costs may not be reduced because it is essential that system development stay current. Development cost for MADD may be

reduced if it can draw upon already available technology at the time of development. Major cost savings will result from the application of more capable, less costly systems.

VI. Optimal Detumbling Sequences

The minimum time optimal detumbling analyses of a distressed space vehicle can be divided into the following areas: constraint on the magnitude of control moment vector and constraint on the magnitude of each component of this vector. These areas may be expressed as

$$(u_1^2 + u_2^2 + u_3^2)^{1/2} \leq M$$

$$|u_k| \leq m_k \qquad k = 1,2,3.$$

The space vehicle is modeled as a rigid body by Euler's moment equations:[6]

$$\begin{aligned} T_1 &= A\dot{\omega}_1 + \omega_2\omega_3 \ (C-B) \\ T_2 &= B\dot{\omega}_2 + \omega_1\omega_3 \ (A-C) \\ T_3 &= C\dot{\omega}_3 + \omega_1\omega_2 \ (B-A) \end{aligned} \tag{32}$$

The objective is to reduce the three angular velocity components to zero in minimum time.

The first type of constraint leads to a fairly simple solution.[11] It turns out that the required orientation of the control moment is opposite to the angular momentum vector and its magnitude is the largest available from the reaction jets. Writing

$$x_k = I_k\omega_k \qquad k = 1,2,3$$

where I_k = moment of inertia about k axis and placing into Euler's moment equations we get

$$\dot{x}_1(t) = \alpha_1 x_2(t)\, x_3(t) + u_1(t)$$

$$\dot{x}_2(t) = \alpha_2 x_3(t)\, x_1(t) + u_2(t) \tag{33}$$

$$\dot{x}_3(t) = \alpha_3 x_1(t)\, x_2(t) + u_3(t)$$

where

$$\alpha_1 = \frac{I_2 - I_3}{I_2 I_3}$$

$$\alpha_2 = \frac{I_3 - I_1}{I_3 I_1}$$

$$\alpha_3 = \frac{I_1 - I_2}{I_2 I_1}$$

The optimal control moment is

$$u_{\text{min time}}(t) = - M \frac{x^*(t)}{||x^*(t)||} \tag{34}$$

where

$$||x^*(t)|| = [x^*_1{}^2(t) + x^*_2{}^2(t) + x^*_3{}^2(t)]^{1/2}$$

and

$x^*(t)$ is the solution of

$$x(t) = f[x(t);t] - M \frac{x(t)}{||x(t)||} \tag{35}$$

starting from $x_i(t_o) = \zeta_i$, $i = 1,2,3$ to origin ($x_i = 0$, $i = 1,2,3$).

For our case we get, for x(t):

$$\dot{x}_1(t) = \alpha_1 \, x_2(t) \, x_3(t) - \frac{M \, x_1(t)}{[x_1^2(t) + x_2^2(t) + x_3^2(t)]^{1/2}}$$

$$\dot{x}_2(t) = \alpha_2 x_3(t) \, x_1(t) - \frac{M \, x_2(t)}{[x_1^2(t) + x_2^2(t) + x_3^2(t)]^{1/2}} \qquad (36)$$

$$\dot{x}_3(t) = \alpha_3 x_1(t) \, x_2(t) - \frac{M \, x_3(t)}{[x_1^2(t) + x_2^2(t) + x_3^3(t)]^{1/2}}$$

These equations were applied to the tumbling MSS caused by collision with the Mark II Orbiter assuming 100% kinetic energy exchange.[1] The principal axis angular velocities at commencement of thrusting were chosen at t = 120 sec. after collision; here the ω_i's are fairly large so as to give a good test to this optimization technique. The angular velocities are 1.150, 1.750 and -0.445 RPM's about 1, 2 and 3 principal axes, respectively. These velocities were brought to near zero in about 7 minutes with the application of a maximum control moment vector magnitude (M) of 3400 Nm (2500 ft-lbs). Figure 20 shows a time history of the principal axis angular velocities during application of the optimum control moment. Figure 21 gives a time history of the body fixed thrusts (lbs) required at point x = -2.17 m (-7.13 ft), y = -.915 m (-3.0 ft) and z = 21.2 m (69.5 ft) to give the necessary

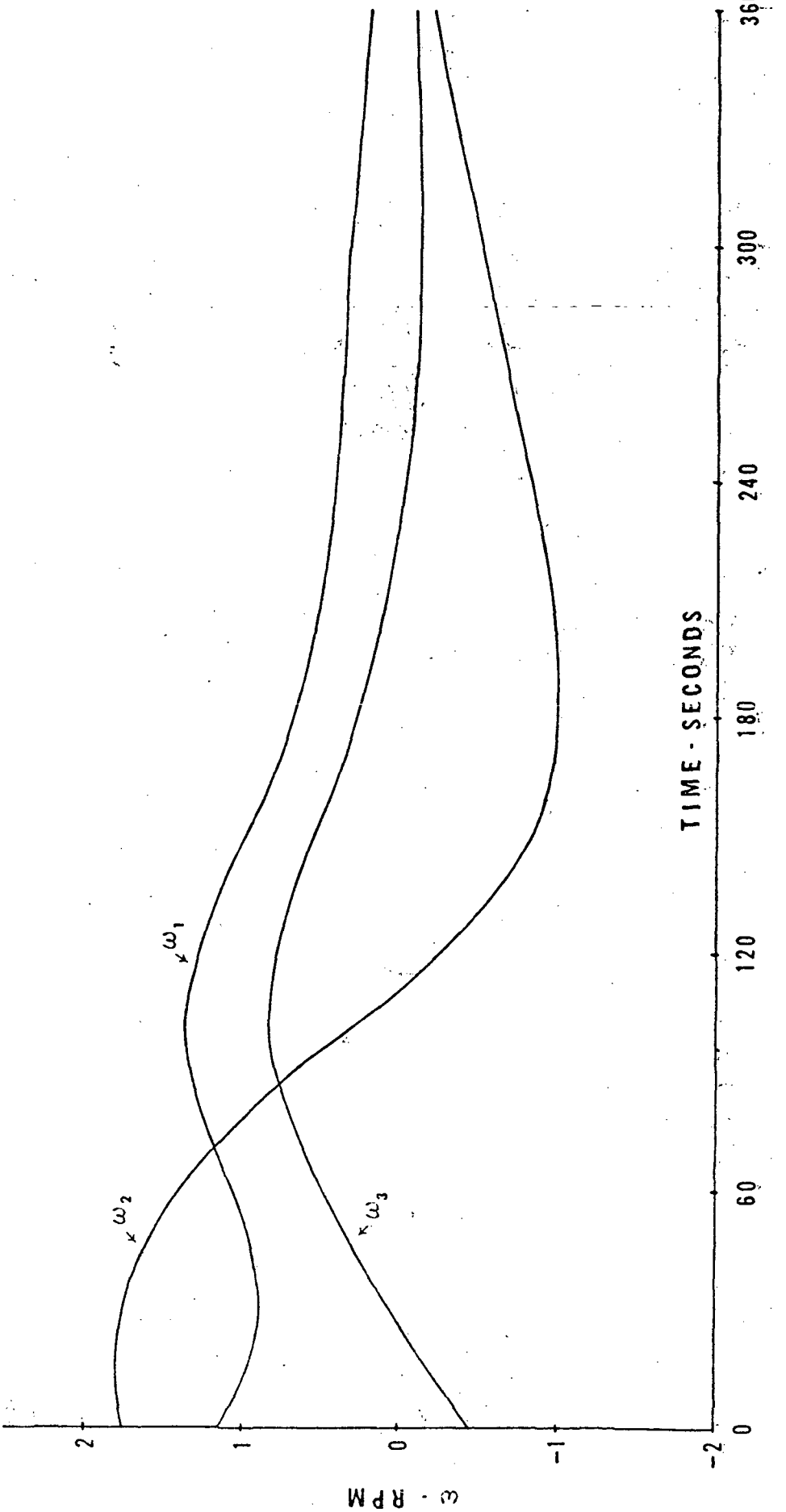

Figure 20. Principal Angular Velocities During Detumbling

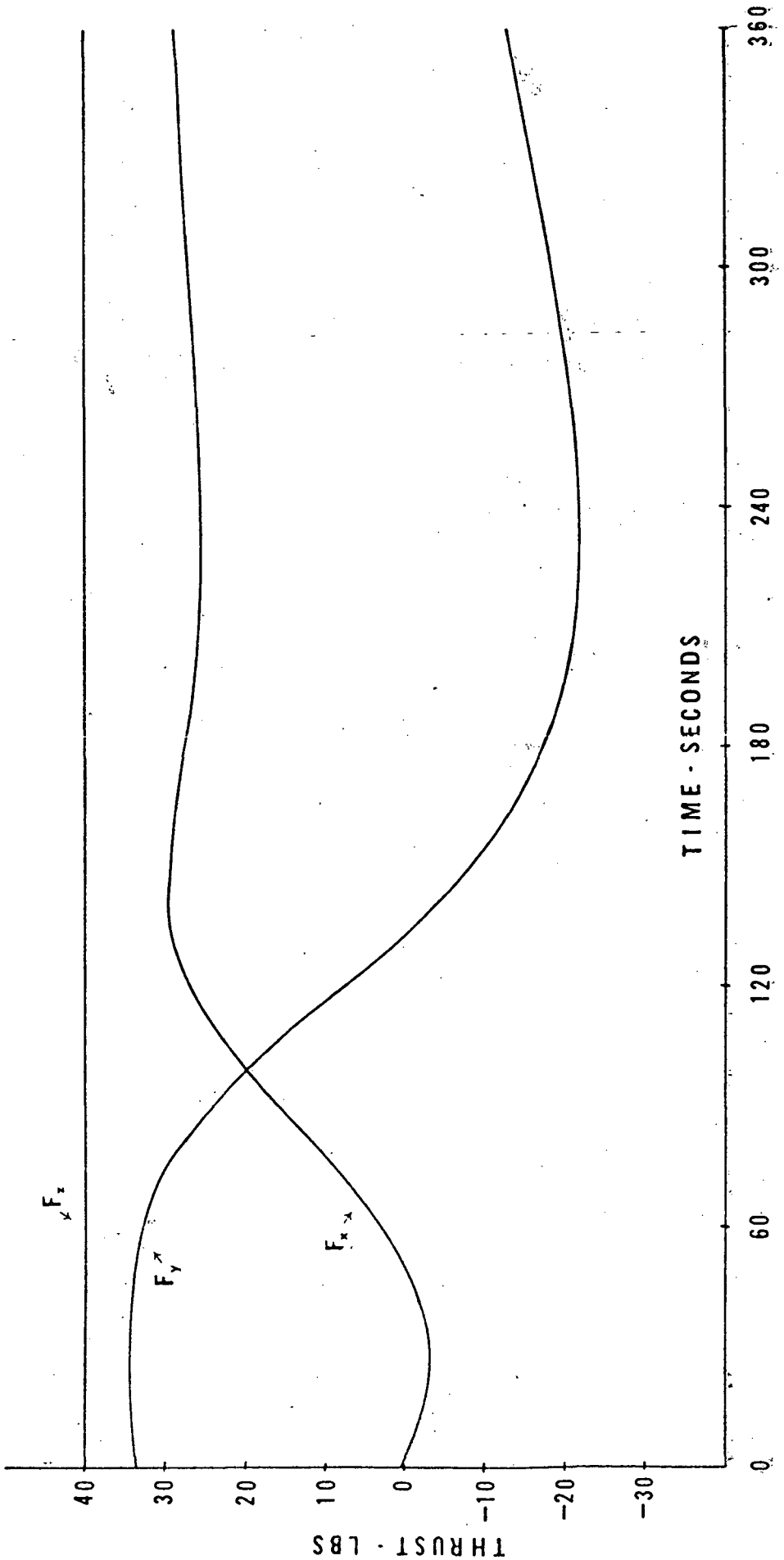

Figure 21. Body Fixed Thrust at X= -2.17m, Y= -.915m, Z= 21.2m for 3400 Nm Max. Torque

3400 Nm (2500 ft-lb) moment directed opposite to the angular momentum vector. With the application of 10,200 Nm (7500 ft-lbs), the MSS is detumbled in 140 sec. Figures 22 and 23 show the results. The x, y, and z coordinates for the thrust application are the same. Assuming I_{sp} = 240 sec, 45.4 Kg (100 lbs) of fuel are used for the 3400 Nm (2500 ft-lbs) case and 56.0 Kg (123 lbs) are used for the 10,200 Nm (7500 ft-lbs) case.

The second type of constraint ($u_i \leq m_i$, i = 1,2,3) present more difficulty in determining the optimum minimum time control moment sequence. In this case, the analysis is not as easily accomplished; the control moment vector is not simply directed opporite to the angular momentum vector. As subsequent analysis will show, the magnitudes of the components (u_i) of the control moment vector (u) will be the largest possible (m_i) - what will change will be the direction of thrust (+, -). This change in directions of thrust (switching times) is, in fact, the major concern in this type of analysis. The equations describing minimum time detumbling for the constraint $u_i \leq m_i$ are as follows:[11,12]

$$\dot{x}_1(t) = \alpha_1 x_2(t)\, x_3(t) + u_1(t)$$

$$\dot{x}_2(t) = \alpha_2 x_3(t)\, x_1(t) + u_2(t) \qquad (37)$$

$$\dot{x}_3(t) = \alpha_3 x_1(t)\, x_2(t) + u_3(t)$$

where

$$x_k(t) = I_k \omega_k(t)$$

$\omega_k(t)$ = angular velocity about k^{th} axis

I_k = moment of inertia about k^{th} axis,

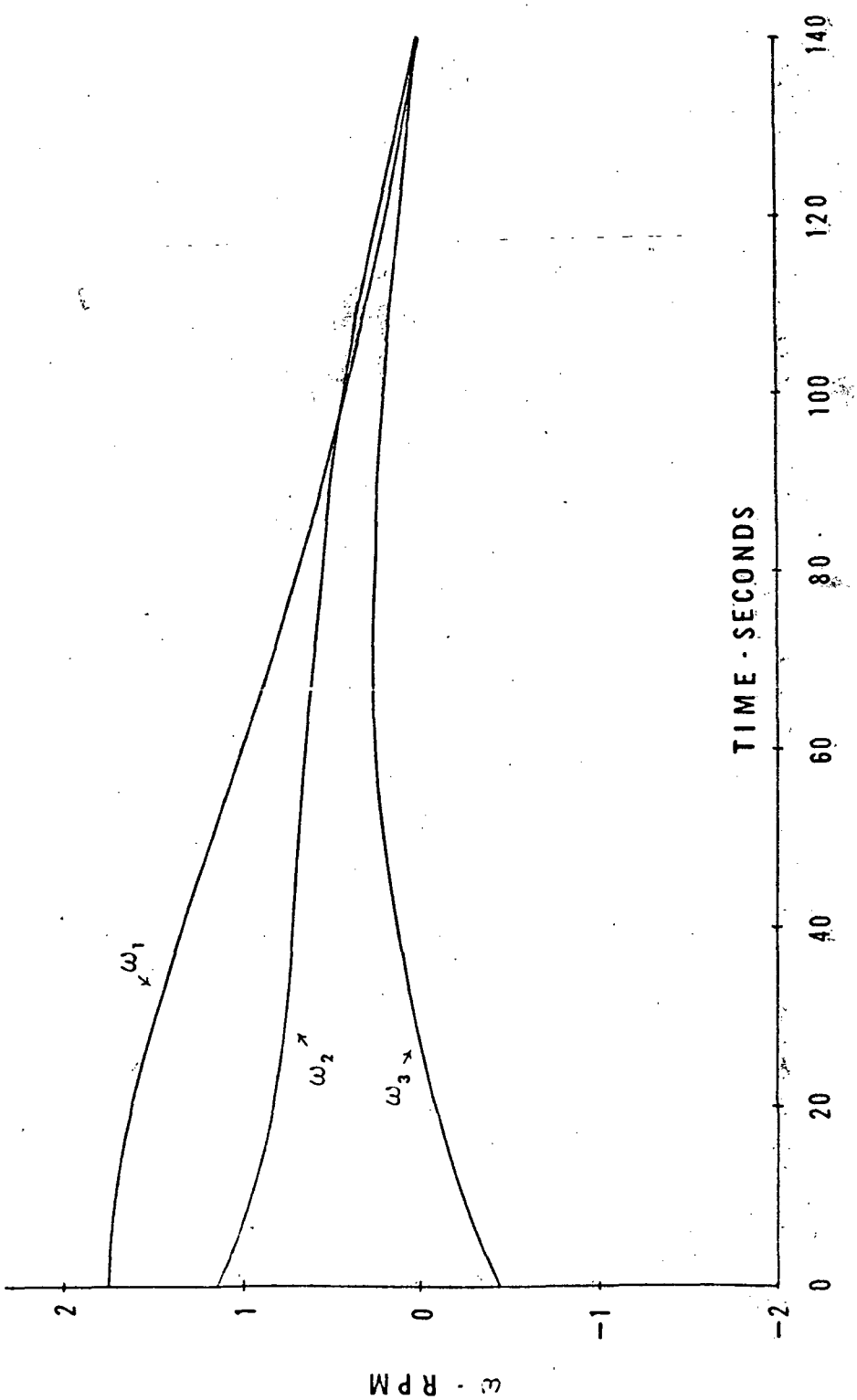

Figure 22. Principal Angular Velocities During Detumbling

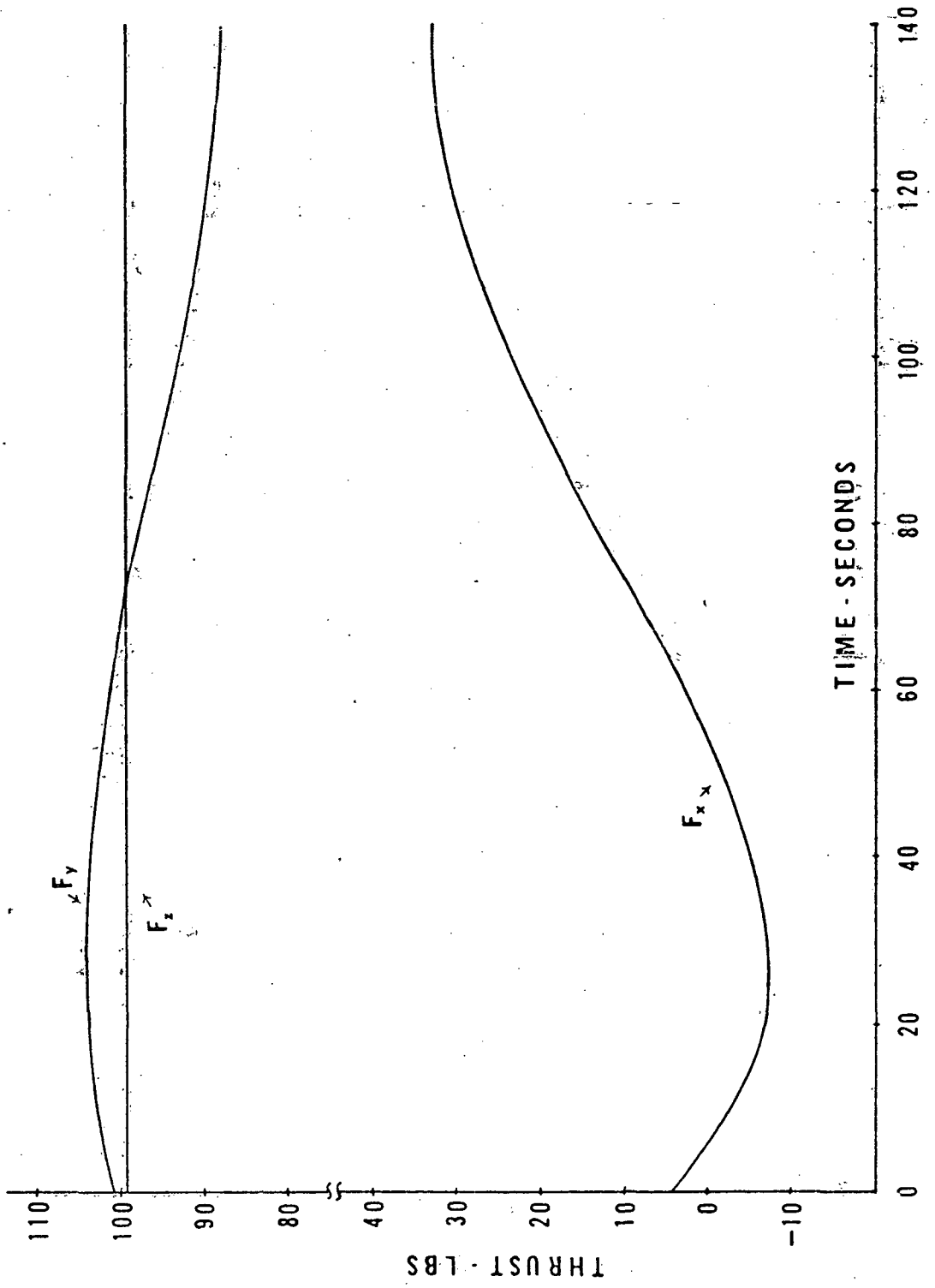

Figure 23. Body Fixed Thrust a X= -2.17m, Y= -.915m, Z= 21.2m for 10,200 Nm Max. Torque

$$
\begin{aligned}
H &= 1 + p_1(t)\,\dot{x}_1(t) + p_2(t)\,\dot{x}_2(t) + p_3\,\dot{x}_3(t) \\
&= 1 + p_1(t)\,\alpha_1 x_2(t)\,x_3(t) + p_1(t)\,u_1(t) \\
&\quad + p_2(t)\,\alpha_2 x_3(t)\,x_1(t) + p_2(t)\,u_2(t) \\
&\quad + p_3(t)\,\alpha_3 x_1(t)\,x_2(t) + p_3(t)\,u_3(t),
\end{aligned} \tag{38}
$$

$$
\dot{p}_k(t) = -\frac{\partial H}{\partial x_k}
$$

which yields

$$
\begin{aligned}
\dot{p}_1(t) &= -\alpha_2 x_3(t)\,p_2(t) - \alpha_3 x_2(t)\,p_3(t) \\
\dot{p}_2(t) &= -\alpha_1 x_3(t)\,p_1(t) - \alpha_3 x_1(t)\,p_3(t) \\
\dot{p}_3(t) &= -\alpha_1 x_2(t)\,p_1(t) - \alpha_2 x_1(t)\,p_2(t)
\end{aligned} \tag{39}
$$

and (for min. H)

$$
u_i(t) = u_{i_{\text{min time}}} = -m_i \operatorname{sgn}\{p_i(t)\} \tag{40}
$$

which gives

$$
\begin{aligned}
u_1(t) &= -m_1 \operatorname{sgn}\{p_1(t)\} \\
u_2(t) &= -m_2 \operatorname{sgn}\{p_2(t)\} \\
u_3(t) &= -m_3 \operatorname{sgn}\{p_3(t)\}\,.
\end{aligned} \tag{41}
$$

As can be seen from the above equations for the control moment components $u_1(t)$, $u_2(t)$ and $u_3(t)$, the control history will be of a bang-bang type; this requires investigation for the switching times. First order gradient techniques may be used to obtain the switching times.[13] However, solutions were not obtained since variable thrusters are available on MADD and the mehtod discussed previously (constraint on the magnitude of the moment vector) should require less fuel to perform an equivalent task. It should be noted that the control history will still be bang-bang even if nonprincipal axis are used since the equations of motion will remain linear in u_i.

VII. Conclusions and Recommendations

Problems related to docking with and detumbling a passive modular space station have been considered here. A MADD concept is proposed as a means to apply controlled external torques to detumble a manned space base without endangering the shuttle and a preliminary design is presented. An operational procedure has been outlined and each subsystem discussed. Appropriate assumptions on mission requirements and constraints were formulated based on expected future programs and developments. Position, attitude, and detumble control systems were developed. As an application the MSS is shown to be detumbled in a few minutes with very small reaction jets. Furthermore, it can be stated that structural limitations of the MSS and Human tolerance are not exceeded by the induced "g" loads, and that the fuel weight is low. The operation of MADD has automatic functions, but the shuttle has command control. The general case (tumbling) has been treated here, but MADD could be used for the spin case as well.

References

1. Kaplan, M. H., "Despinning and Detumbling Satellites in Rescue Operations," presented at the Fifth Space Rescue Symposium, Vienna, Austria, October 1972.

2. Layton, J. P. and Grey, J., "New Space Transportation Systems an AIAA Assessment," January 1973.

3. Kendrick, J. B., "TRW Space Data," TRW Systems Group, TRW Inc., 1967, p. 67.

4. Wyman, C. L., "Test Performance of an Experimental Laser Radar for Rendezvous and Docking," J. Spacecraft and Rockets, Vol. 5, No. 4, April 1968, pp. 430-433.

5. Eggleston, J. M. and Beck, H. D., "A Study of the Position and Velocities of a Space Station and Ferry Vehicle during Rendezvous and Return," NASA TR R-87, 1961.

6. Thompson, W. T., Introduction to Space Dynamics, John Wiley and Sons, Inc., New York, 1963.

7. Kuo, B. C., Automatic Control Systems, Prentice-Hall, Inc., N.J., 1967.

8. DiStefano, J. J., Stubberud, A. R. and Williams, I. J., Feedback and Control Systems, McGraw-Hill, Inc., New York, 1967.

9. Greensite, A. L., "Attitude Control in Space," Analysis and Design of Space Vehicle Flight Control Systems, Vol. XII, NASA CR-831, Washington, D.C. August 1967.

10. Moran, F. J. and Dishman, B. H., "Air Bearing Table Mechanization and Verification of a Spacecraft Wide Angle Attitude Control System," J. Spacecraft and Rockets, Vol. 7, No. 7, July 1970, pp. 819-825.

11. Athans, M. and Falb, P. L., Optimal Control, McGraw-Hill, Inc., New York, 1966.

12. Bryson, A. E., Jr. and Ho, Yu-Chi., Applied Optimal Control, Ginn and Co., Mass., 1969.

13. Denham, W. F. and Bryson, A. E., Jr., "Optimal Programming Problems with Inequality Constraints II: Solution by Steepest-Ascent," AIAA Journal, Vol. 2, No. 1, January 1964, pp. 25-34.